JOURNAL OF PETROLOGY | VOLUME 48 | NUMBER 1 | PAGES 79–111 | 2007 | doi:10.1093/petrology/egl055

Hybridization of a Shallow 'I-type' Granitoid Pluton and its Host Migmatite by Magma-Chamber Wall Collapse: the Tokuwa Pluton, Central Japan

SATOSHI SAITO[1], MAKOTO ARIMA[1]* AND TAKASHI NAKAJIMA[2]

[1]GEOLOGICAL INSTITUTE, GRADUATE SCHOOL OF ENVIRONMENT AND INFORMATION SCIENCES, YOKOHAMA NATIONAL UNIVERSITY, TOKIWADAI, HODOGAYA-KU, YOKOHAMA 240-8501, JAPAN

[2]GEOLOGICAL SURVEY OF JAPAN, 1-1-1 HIGASHI, TSUKUBA 305-8567, JAPAN

RECEIVED NOVEMBER 20, 2003; ACCEPTED SEPTEMBER 1, 2006; ADVANCE ACCESS PUBLICATION NOVEMBER 7, 2006

The Miocene Tokuwa pluton of 'I-type' granitoid affinity was emplaced discordantly into a Cretaceous to Paleogene accretionary complex and induced a contact aureole in which various thermally metamorphosed rocks were developed, including hornfels, metatexite, diatexite and cordierite-bearing tonalite (Crd-tonalite) of 'S-type' granite affinity. The thermally metamorphosed rocks show low-pressure reaction textures culminating in partial melting. Peak P–T conditions of ~3 kbar at ~780°C are estimated on the basis of the TWQ thermobarometer for the garnet-bearing rocks. The rocks in the contact aureole exhibit a gradual transition from hornfels, through metatexite and diatexite to Crd-tonalite. The Sr-isotopic composition at the time of Tokuwa pluton emplacement at 12 Ma decreases systematically from metatexite (0·7100–0·7112) through diatexite (0·7078–0·7094) to Crd-tonalite (0·7067–0·7068); this trend is interpreted in terms of mixing between the Tokuwa magma and the aureole migmatites. The field relationships, geochemical data, and isotopic data collectively suggest that the emplacement of the Tokuwa pluton triggered partial melting of the surrounding metasedimentary rocks. Subsequent hybridization of the Tokuwa magma with the metatexite in variable proportions produced the Crd-tonalite and diatexite. The hybridization was caused by invasion of the Tokuwa magma into the migmatite zone, accompanied by gravitational collapse of the previously crystallized wall of the magma chamber. The data presented demonstrate that even a relatively low-temperature, shallow, 'I-type' granitoid pluton can induce contact anatexis and hybrid 'S-type' granitoid formation at the intrusive contact.

KEY WORDS: *contact metamorphism; hybridization; magma–host-rock interaction; migmatite; 'S-type' granitoid*

INTRODUCTION

To understand the petrogenetic history of a granitic pluton it is essential to decipher not only the processes in the source region, but also the extent of the interaction of magma with its country rocks at the level of emplacement. It is well documented that granitoid magmas intruding partially melted middle crust interact with their anatectic host-rocks, forming hybrid facies along the contact (e.g. Ugidos & Recio, 1993; Greenfield *et al.*, 1996). However, in the case of shallow-level granitoid plutons evidence for contact anatexis induced by the plutons is scarce and occurs only where H_2O is available to facilitate melting of the host-rocks. This is mainly a consequence of the relatively low temperature of the initial granitoid magmas, which are unlikely to cause extensive melting of country rocks that were initially at low temperature. Although contact anatexis around shallow-level granitoid plutons has been documented in some contact aureoles (e.g. Ballachulish aureole: Pattison & Harte, 1988; Holness & Clemens, 1999; Onawa aureole: Symmes & Ferry, 1995; Marchildon & Brown, 2001; Goat Ranch migmatite complex: Zeng *et al.*, 2005*a*, 2005*b*), the mechanism of interaction between granitoid magmas

*Corresponding author. Telephone: +81-45-339-3354. Fax: +81-45-339-3264. E-mail: arima@server2.edhs.ynu.ac.jp

© The Author 2006. Published by Oxford University Press. All rights reserved. For Permissions, please e-mail: journals.permissions@oxfordjournals.org

Downloaded from http://petrology.oxfordjournals.org/ by guest on June 28, 2012

and their anatectic host-rocks has received little attention in the literature.

The Miocene Tokuwa pluton is of 'I-type' granitoid affinity (Sato & Ishihara, 1983; Shimizu, 1986; Takahashi, 1989; Sato, 1991) and is exposed in the Izu arc collision zone, central Japan. The pluton exhibits a thermal aureole in which the rocks range from low-grade hornfels to migmatite; the migmatites locally exhibit a gradual transition from metatexite through diatexite to cordierite-bearing tonalite. The objectives of this study are (1) to describe the field relationships between the Tokuwa pluton and its host-rocks through the contact aureole, (2) to estimate the P–T conditions of emplacement of the Tokuwa pluton, and (3) to discuss the petrogenetic processes involved in magma–host-rock interaction within the contact aureole, based on isotopic and geochemical constraints.

GEOLOGICAL BACKGROUND

The Izu Collision Zone (Taira *et al.*, 1989; Soh *et al.*, 1991) is located near the Boso triple junction (Ogawa *et al.*, 1989), where the northern Izu–Bonin–Mariana (IBM) arc system has been colliding with the Honshu arc since the middle Miocene (*c.* 15 Ma) (Niituma, 1989; Soh *et al.*, 1991; Takahashi & Saito, 1997; Aoike, 1999) (Fig. 1a). The IBM arc is an immature intra-oceanic island arc in contrast to the mature Honshu arc. Neogene granitoid plutons are widely exposed in the Izu Collision Zone (Fig. 1a). The Kofu granitic complex (KGC) is the largest pluton among the Neogene granitoids in Japan and consists of several intermediate to felsic plutons including the Kinpusan, Tokuwa, Tonogi and Ashigawa plutons (Sato & Ishihara, 1983; Shimizu, 1986; Takahashi, 1989; Sato, 1991; Saito *et al.*, 2004) (Fig. 1b). The Kinpusan pluton (northwestern part of KGC) consists of weakly peraluminous biotite-bearing granite, whereas the central part (Tokuwa pluton) predominantly consists of metaluminous hornblende–biotite-bearing granodiorite. The southern part of the KGC (Ashigawa and Tonogi plutons) is composed mainly of metaluminous hornblende-bearing tonalite and trondhjemite.

The Tokuwa pluton is the largest intrusive unit of the KGC. It intrudes discordantly into a Cretaceous to Paleogene accretionary complex that is composed mainly of shale and sandstone (Shimanto Belt, Fig. 2a). The internal part of the Tokuwa pluton corresponds to the magnetite-series of Ishihara (1977), but the thick external part is composed mainly of ilmenite-series rocks (Fig. 2a). This external part is characterized by an abundance of sedimentary xenoliths and has been interpreted as a marginal facies generated by magma–country rock interaction (Shimizu, 1986; Takahashi, 1989; Sato, 1991). The main body of the Tokuwa pluton is medium-grained (~2 mm grain size) and consists principally of plagioclase, quartz, K-feldspar, amphibole, biotite, and opaque minerals. It includes rocks ranging in composition from quartz-diorite, tonalite and granodiorites to granite (Fig. 3). The relatively mafic facies (<19 modal % Qtz, <1 modal % Kfs) are restricted to the external part; these have a large proportion of poikilitic hornblende (20–30 modal %) containing euhedral to subhedral plagioclase grains.

K–Ar dating for the KGC yields ages ranging from 15·7 to 7·4 Ma (Kawano & Ueda, 1966; Shibata *et al.*, 1984; Saito *et al.*, 1997), linking their genesis to the IBM arc–Honshu arc collision event. Although a number of petrological studies have been performed on the KGC, the petrogenesis of these plutons is as yet not fully understood. Sato (1991) suggested, based on Sr, O and S isotope data, that the range of petrographic and geochemical variations observed in the KGC was caused by variable degrees of assimilation of sedimentary materials into mantle-derived mafic magmas. In contrast, Saito *et al.* (2004) suggested that the southern plutons of the KGC (Ashigawa and Tonogi plutons) were formed by crystal fractionation processes from an intermediate parental magma that originated from the anatexis of basaltic crustal source materials. According to these workers, the collision process between the IBM and Honshu arcs caused the crustal anatexis that led to the formation of the Ashigawa and Tonogi plutons.

ANALYTICAL METHODS

Mineral analyses were carried out using an automated energy-dispersive electron microprobe (LINK QX2000J system) at the Geological Institute of Yokohama National University. The operating conditions were 15 kV and 0·155 nA on a cobalt standard. Data were processed using a LINK ZAF-4/FLS correction program. Representative mineral compositions are given in Table 1. Mineral abbreviations follow Kretz (1983).

Major and trace element compositions were determined for thermally metamorphosed rocks in the contact aureole and granitoids from the Tokuwa pluton. The powder samples for whole-rock analysis were carefully prepared from 0·1–0·5 kg rock samples of the hornfels. The metatexite, diatexite, Crd-tonalite and granitoids are fine- to medium-grained rocks (<3 mm) and the sample powders were prepared from 0·2–1·0 kg rock samples. The analyzed samples of leucosome and schollen (10–50 g) were extracted from the diatexite. Crushed samples were pulverized using an agate ball mill. Major and trace element analyses were determined by X-ray fluorescence (XRF) (RIGAKU RIX-3000) at the National Institute of Polar Research, Japan. The analytical procedure followed the methods of Motoyoshi & Shiraishi (1995), Motoyoshi *et al.* (1996) and Yamada *et al.* (1997).

Sr-isotopic compositions for several representative samples of various rock types were determined using a

Downloaded from http://petrology.oxfordjournals.org/ by guest on June 28, 2012

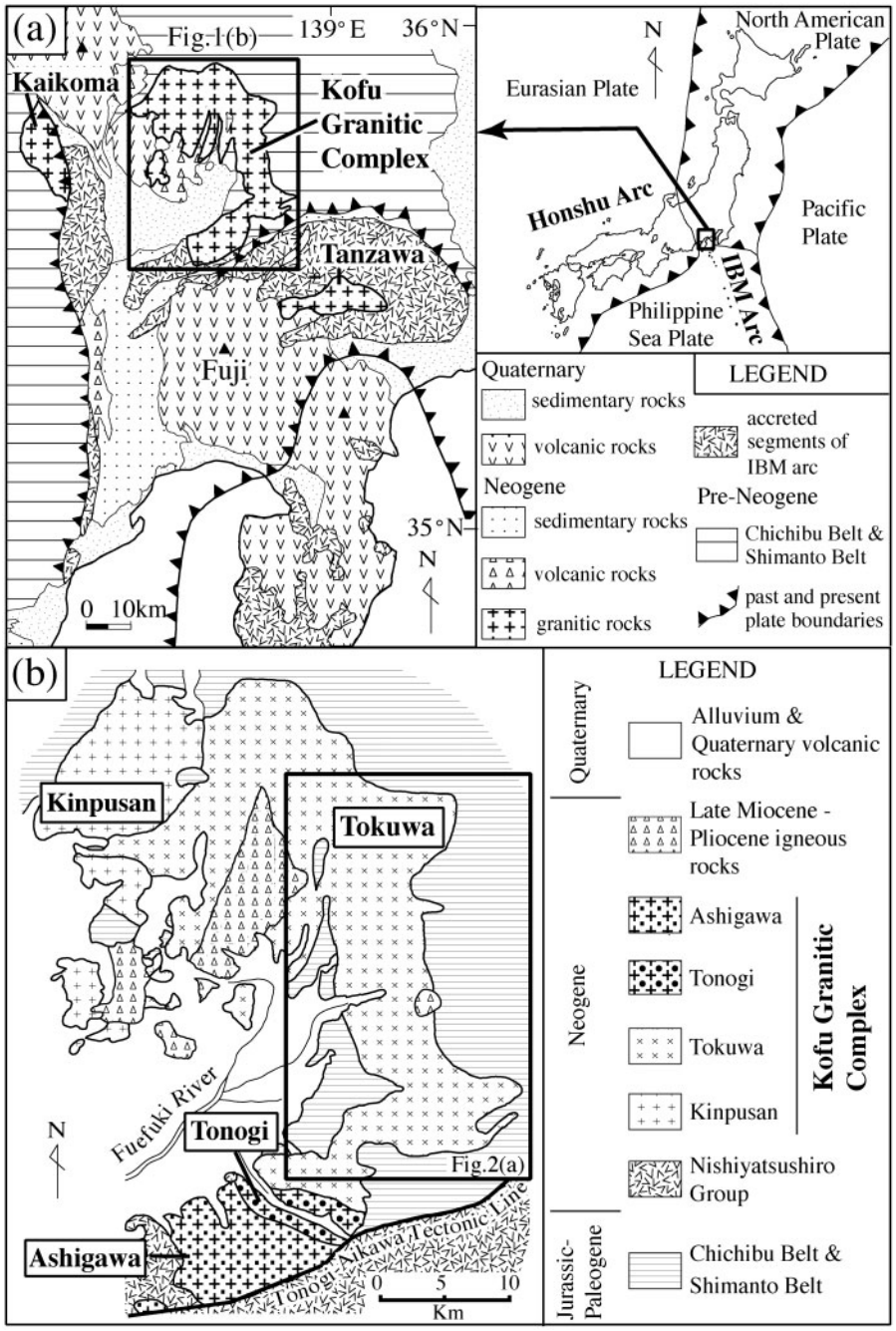


Fig. 1. (a) Geological map of the Izu Collision Zone (modified after Takahashi & Saito, 1997). (b) Geological map of the Kofu Granitic Complex (modified after Sato & Ishihara, 1983; Takahashi, 1989; Sato, 1991; Saito *et al.*, 2004). Rectangle indicates the location of Fig. 2a.

VG Sector mass spectrometer at the Geological Survey of Japan, following the procedure described by Nakajima *et al.* (1990). $^{87}Sr/^{86}Sr$ ratios were normalized to $^{86}Sr/^{88}Sr = 0{\cdot}1194$. Repeated analyses of the NBS987 standard during this study gave a $^{87}Sr/^{86}Sr$ of $0{\cdot}71025 \pm 0{\cdot}00002$ (1σ). As the K–Ar biotite age of the Tokuwa pluton in the studied area is about 12 Ma (Saito *et al.*, 1997), 'initial' Sr-isotopic ratios (SrI) at a time of the Tokuwa pluton emplacement were recalculated back to 12 Ma. Representative whole-rock and Sr-isotope compositions are given in Table 2. Modal proportions (%) of minerals determined by point counting of thin

Downloaded from http://petrology.oxfordjournals.org/ by guest on June 28, 2012

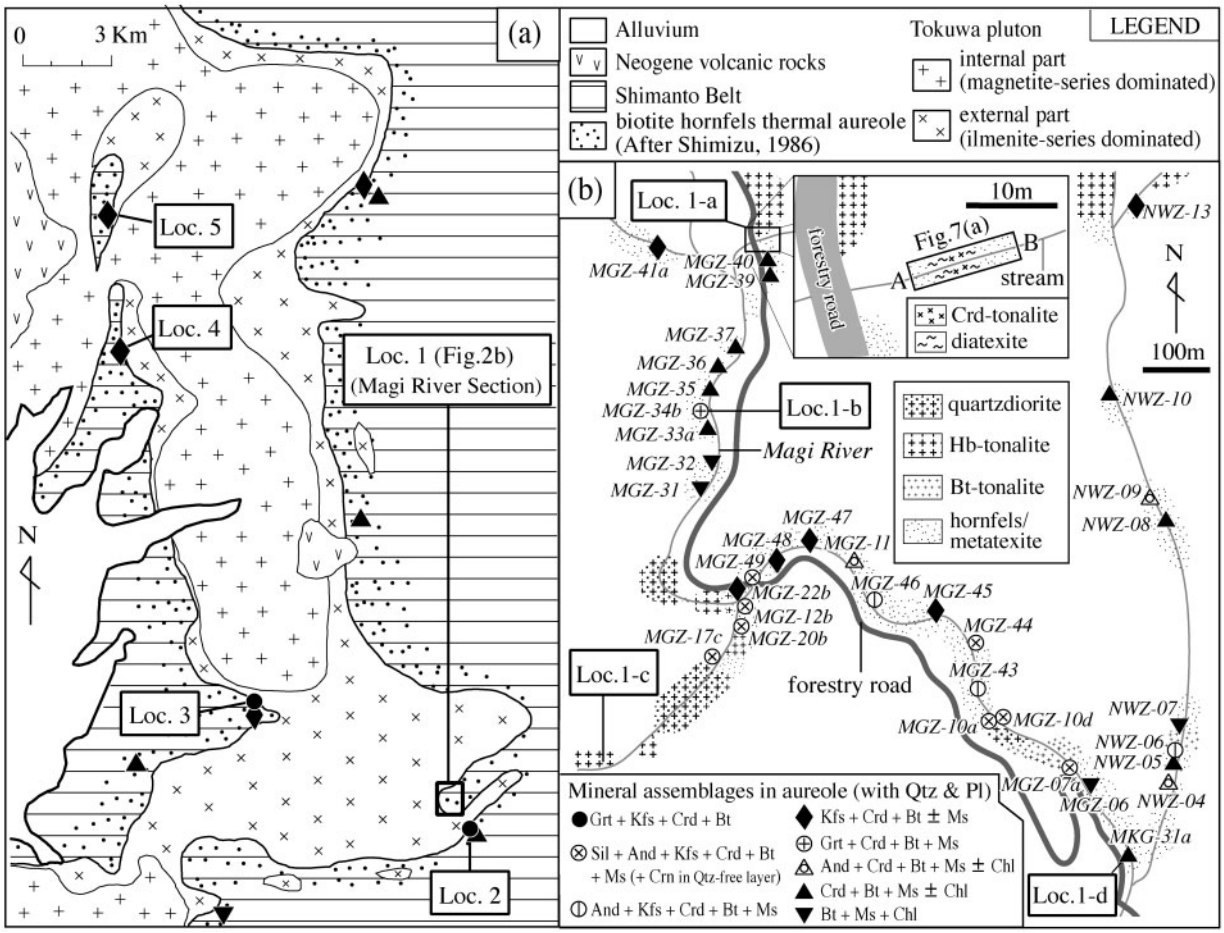


Fig. 2. (a) Geological map of the Tokuwa pluton (modified after Shimizu, 1986; Sato, 1991; Ozaki *et al.*, 2002) showing the contact aureole and the migmatite localities (Loc. 1–5). Mineral assemblages in pelitic rocks in the contact aureole are indicated. The internal zone of the Tokuwa pluton consists of magnetite-series granitoids with a wide external zone composed mainly of ilmenite-series granitoids (Sato, 1991). (b) Route map of Loc. 1 (Magi River section). Crd-tonalite, diatexite and metatexite are exposed along a stream at Loc. 1-a. Pelitic mineral assemblages and sample numbers studied are indicated.

sections are also listed in Table 2 for granitoids from the Tokuwa pluton, the diatexite and the Crd-tonalite.

THE TOKUWA CONTACT AUREOLE

A metamorphic thermal aureole (1–3 km wide) defined by the biotite-in isograd (Shimizu, 1986) is developed around the Tokuwa pluton (Fig. 2). Hornfels is the dominant rock type in the aureole. The hornfels consists of pelitic and quartzofeldspathic layers, which are inferred to represent original sedimentary bedding. Towards the intrusive contact the aureole rocks exhibit progressive changes in their mineral assemblage summarized as: Bt + Ms + Chl + Qtz + Pl, Crd + Bt + Ms + Qtz + Pl ± Chl, And + Crd + Bt + Ms + Qtz + Pl ± Chl, Grt + Crd + Bt + Ms + Qtz + Pl, Kfs + Crd + Bt + Qtz + Pl ± Ms, And + Kfs + Crd + Bt + Ms + Qtz + Pl, Sil + And + Kfs + Crd + Bt + Ms + Pl ± Qtz ± Crn, and Grt + Kfs + Crd + Bt + Qtz + Pl (Table 3). Representative microstructures in the hornfels are shown in Fig. 4.

Metatexites are exposed in the aureole within ~15 m of the intrusive contact (Loc. 1, 2, 3, 4 and 5; Fig. 2; Table 3). These have a layered appearance consisting of mica-rich pelitic and quartz-rich psammitic layers, similar to the hornfels. Although the mineral assemblage of the metatexites is comparable with that in the hornfels, the metatexite has distinct petrographic characteristics indicative of partial melting, which were not identified in the hornfels. These include: (1) the presence of chemically zoned plagioclase; (2) the development of thin interstitial films composed of quartz and feldspars along grain boundaries (see Sawyer, 1999); (3) development of euhedral crystals of quartz, cordierite, plagioclase and/or K-feldspar (Fig. 5a) (see Vernon & Collins, 1988).

Downloaded from http://petrology.oxfordjournals.org/ by guest on June 28, 2012

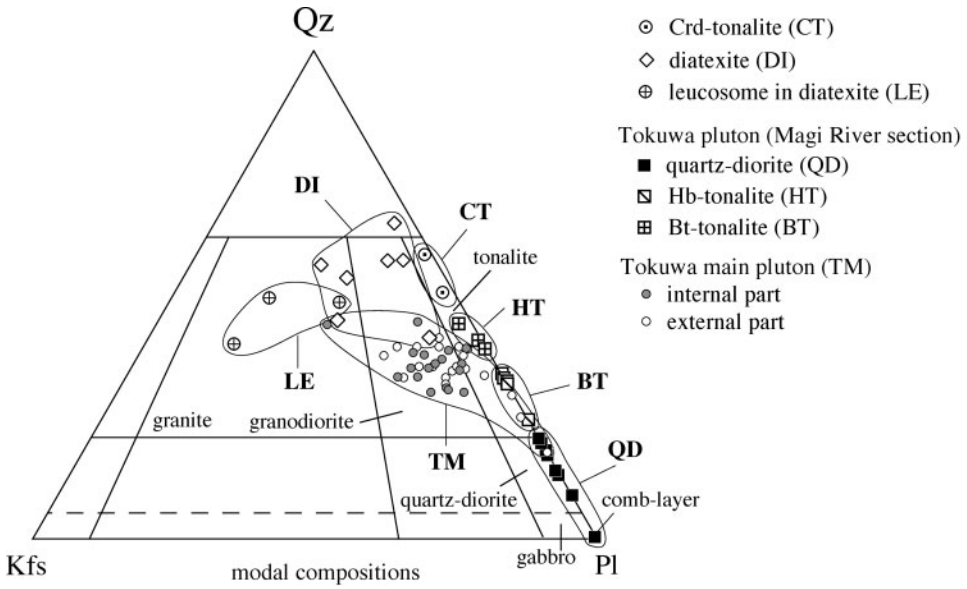


Fig. 3. Modal Qtz–Pl–Kfs compositions of the Crd-tonalite, diatexite, leucosome and Tokuwa pluton. The classification of granitoids is after LeBas & Streckeisen (1991).

Contact aureole and Tokuwa pluton contact in the Magi River section

Along the Magi River, in the southeastern part of the contact aureole around the Tokuwa pluton (Loc. 1, Fig. 2b), there are extensive exposures of hornfels and metatexite. The intrusive contact of the Tokuwa pluton with the metatexites is sharp and well exposed (Fig. 6a). Dykes (50 cm to 2 m in width) derived from the Tokuwa pluton are locally present, cutting across the host-rock structures (Fig. 6b). Aplitic veins (~50 cm width) cut both the host-rock structures and the dykes (Fig. 6b). Thin quartz veins (<1 cm width) occur in the hornfels and are concordant with the structures in the host-rocks, although in some places they cut the layering.

The Tokuwa pluton exposed in the Magi River section shows a wide range of petrographic variation that can be grouped into three main facies: (1) medium- to fine-grained, hornblende–biotite-bearing tonalite (Hb-tonalite); (2) fine-grained, hornblende-free, biotite-bearing porphyritic tonalite (Bt-tonalite); (3) medium- to fine-grained, hornblende–biotite-bearing quartz-diorite, locally developing a comb-layering structure (see Moore & Lockwood, 1973). The Hb-tonalite consists of plagioclase (54–65 modal %; $An_{27–79}$), quartz (17–29 modal %), hornblende (5–21 modal %), biotite (6–10 modal %), and opaque minerals (<1 modal %) and overlaps the field of tonalite (Figs 3 and 6c). Aligned plagioclase laths are a characteristic feature of the fine-grained Hb-tonalite (Fig. 6d), suggesting a cumulate origin. This fine-grained type of Hb-tonalite is restricted to the marginal part of the pluton (up to 100 m from the intrusive contact). In the vicinity of the contact (~1 m from the country rocks), the fine-grained Hb-tonalite contains orthopyroxene xenocrysts, which in places are surrounded by cummingtonite.

The Bt-tonalite consists of plagioclase (46–54 modal %; $An_{23–80}$), quartz (34–40 modal %), biotite (10–13 modal %) and opaque minerals (<1 modal %). In the Qtz–Kfs–Pl diagram, this rock overlaps with the field for tonalite (Fig. 3). The Bt-tonalite is characterized by a porphyritic texture consisting of oscillatory-zoned ($An_{23–80}$) phenocrystic plagioclase (0·5–1 mm in diameter) in a fine-grained groundmass (Fig. 6e). The plagioclase in the groundmass is normally zoned ($An_{20–67}$). The rock contains angular xenoliths (1–30 cm in diameter) of fine-grained metapelite (<0·1 mm grain size) (Fig. 6f), which contain the mineral assemblage biotite + plagioclase ± muscovite ± quartz ± andalusite ± corundum. The petrographic characteristics of the pelitic xenoliths are similar to those of the hornfels occurring within the contact aureole.

The quartz-diorite is a hornblende-rich, medium- to fine-grained rock (Fig. 3) consisting of plagioclase (52–62 modal %; $An_{28–87}$), hornblende (18–33 modal %), biotite (2–12 modal %), quartz (5–13 modal %) and opaque minerals (<3 modal %) (Fig. 6g). This rock exhibits cumulate textures defined by preferentially oriented plagioclase and large (up to 2 cm in diameter) poikiloblastic hornblende crystals. In places, a comb-layering structure is developed in the quartz-diorite (Fig. 6h). The comb-layers have a gabbroic composition (Fig. 3) and consist of long (up to 1 cm length) laths of plagioclase crystals (~48 modal %; $An_{74–87}$), coarse hornblende crystals (~50 modal %), opaque minerals (~2 modal %), and minor quartz and biotite grains (<1 modal %).

Downloaded from http://petrology.oxfordjournals.org/ by guest on June 28, 2012

Table 1: Representative electron microprobe analyses of minerals from hornfels, migmatites, Crd-tonalite, and the Tokuwa pluton

Rock type:	Hornfels (Loc. 1-b)						Metatexite—mesosome (Loc. 2)					Metatexite—mesosome (Loc. 3)						Metatexite—mesosome (Loc. 1-a)				Metatexite—leucosome (Loc. 1-a)			
Sample no.:	MGZ-34b						MGZ-03a					HIK-13						MKG-33d				MKG-33i			
Mineral:	Ms*	Bt*	Crd*	Grt*	Pl core	Pl rim	Bt*	Crd*	Grt*	Pl core	Pl rim	Bt*	Crd*	Grt core*	Grt rim*	Pl core	Pl rim	Bt	Crd	Pl core	Pl rim	Bt	Crd	Pl core	Pl rim
Oxides (wt %)																									
SiO_2	46·30	36·40	47·88	36·28	61·98	62·55	35·6	48·35	35·99	60·45	67·53	36·79	47·83	37·19	37·05	57·80	60·30	36·09	49·40	62·07	64·50	37·09	48·96	62·29	63·18
TiO_2	—	3·35	—	—	—	—	3·72	—	—	—	—	4·18	—	—	—	—	—	4·01	—	—	—	4·97	—	—	—
Al_2O_3	35·50	19·48	32·73	20·52	23·87	24·37	18·66	33·23	20·75	24·51	20·21	18·38	33·69	21·57	21·14	26·22	24·91	18·86	33·02	23·66	22·66	18·36	32·82	23·98	23·35
FeO(total)	1·78	22·04	10·85	32·46	—	—	21·98	9·52	30·21	—	—	19·83	9·19	27·51	27·27	0·48	—	19·75	9·45	—	—	19·17	10·16	—	—
MnO	—	—	0·98	7·83	—	—	0·44	1·35	9·40	—	—	—	1·47	8·59	9·97	—	—	—	0·72	—	—	—	—	—	—
MgO	0·83	6·91	6·30	1·84	—	—	7·22	6·37	2·41	—	—	7·37	6·73	3·62	2·85	—	—	7·35	6·49	—	—	7·19	6·69	—	—
CaO	—	—	—	0·89	5·04	4·99	—	—	0·93	6·05	0·51	—	—	1·46	1·38	7·55	5·28	—	—	5·16	2·93	—	—	4·52	3·19
Na_2O	0·61	—	—	—	8·65	8·64	—	—	—	8·32	11·61	—	—	—	—	7·22	8·38	—	—	8·67	9·61	—	0·34	9·06	9·73
K_2O	9·82	8·90	—	—	0·21	0·32	8·64	—	—	—	0·12	9·07	—	—	—	0·21	0·14	9·79	—	—	—	8·97	—	—	0·26
Total	94·84	97·06	98·73	99·82	99·74	100·87	96·26	98·82	99·69	99·33	99·98	95·61	98·91	99·93	99·67	99·48	99·01	95·85	99·08	99·56	99·70	95·75	98·97	99·85	99·71
O =	22	22	18	12	8	8	22	18	12	8	8	22	18	12	12	8	8	22	18	8	8	22	18	8	8
Si	6·18	5·46	4·98	2·99	2·75	2·75	5·41	5·00	2·95	2·71	2·96	5·56	4·94	2·98	3·00	2·60	2·70	5·47	5·07	2·76	2·84	5·57	5·04	2·76	2·80
Ti	—	0·38	—	—	—	—	0·43	—	—	—	—	0·47	—	—	—	—	—	0·46	—	—	—	0·56	—	—	—
Al	5·58	3·44	4·02	1·97	1·25	1·26	3·34	4·05	2·00	1·29	1·04	3·27	4·10	2·04	2·01	1·39	1·32	3·37	3·99	1·24	1·18	3·25	3·98	1·25	1·22
Fe	0·20	2·76	0·94	2·18	—	—	2·79	0·82	2·07	—	—	2·50	0·79	1·84	1·84	0·02	—	2·50	0·81	—	—	2·41	0·87	—	—
Mn	—	—	0·09	0·56	—	—	0·06	0·12	0·65	—	—	—	0·13	0·58	0·68	—	—	—	0·06	—	—	—	—	—	—
Mg	0·17	1·55	0·98	0·26	—	—	1·64	0·98	0·30	—	—	1·66	1·04	0·43	0·35	—	—	1·66	1·00	—	—	1·61	1·03	—	—
Ca	—	—	—	0·07	0·24	0·23	—	—	0·08	0·29	0·02	—	—	0·13	0·12	0·36	0·25	—	—	0·25	0·14	—	—	0·21	0·15
Na	0·16	—	—	—	0·74	0·74	—	—	—	0·72	0·99	—	—	—	—	0·63	0·73	—	—	0·75	0·82	—	0·07	0·78	0·83
K	1·67	1·70	—	—	0·01	0·02	1·67	—	—	—	0·01	1·75	—	—	—	0·01	0·01	1·89	—	—	—	1·72	—	—	0·01
Total	13·95	15·29	11·01	8·03	5·00	5·00	15·34	10·97	8·05	5·01	5·02	15·20	11·01	8·00	8·00	5·01	5·01	15·35	10·93	5·00	4·98	15·12	10·99	5·00	5·01

Downloaded from http://petrology.oxfordjournals.org/ by guest on June 28, 2012

Rock type:	Diatexite—matrix				Diatexite—leucosome				Diatexite-schollen				Diatexite—clot			Crd-tonalite				Bt-tonalite (Loc. 1)		
Sample no.:	MKG-23d				MG-het-c-leu-4				MG-het-c-pf				MGZ-35a-A			MKG-23c				MGZ-08c		
Mineral:	Bt	Crd	Pl-core	Pl-rim	Bt	Crd	Pl-core	Pl-rim	Bt	Crd	Pl-core	Pl-rim	Bt	Pl-core	Pl-rim	Bt	Crd	Pl-core	Pl-rim	Bt	Pl-core	Pl-rim
Oxides (wt %)																						
SiO_2	35·65	48·47	45·35	62·60	36·27	48·69	47·89	62·55	36·41	48·40	60·70	61·23	36·46	46·60	59·42	35·44	48·78	46·29	62·38	36·02	48·01	61·31
TiO_2	4·64	—	—	—	4·72	—	—	—	4·62	—	—	—	0·40	—	—	2·22	—	—	—	3·48	—	—
Al_2O_3	18·30	33·36	35·53	23·62	18·49	32·40	34·05	23·73	18·38	33·67	24·87	24·01	20·69	34·70	25·84	19·45	33·06	34·82	23·58	16·67	33·97	23·68
FeO(total)	18·73	8·49	—	—	20·94	9·65	—	—	20·30	9·98	—	—	19·27	—	—	20·08	9·34	—	—	18·27	—	0·75
MnO	—	0·73	—	—	—	0·87	—	—	0·42	—	—	—	—	—	—	0·66	0·48	—	—	0·44	—	—
MgO	8·38	7·14	—	—	6·76	6·73	—	—	7·74	6·78	—	—	11·11	—	—	8·55	6·95	—	—	10·85	—	—
CaO	—	—	17·18	4·22	—	—	15·42	3·86	—	—	5·32	4·97	—	17·57	7·05	—	—	16·75	4·68	—	16·23	4·71
Na_2O	0·88	0·74	1·13	9·24	0·38	—	2·15	9·17	—	—	8·16	9·00	—	1·31	7·54	0·74	0·42	1·64	8·64	—	2·20	8·51
K_2O	9·10	—	0·21	—	9·08	—	—	0·29	9·08	—	0·17	—	8·24	—	0·23	8·83	—	—	0·42	9·46	—	0·21
Total	95·68	98·93	99·40	99·68	96·64	98·34	99·51	99·60	96·95	98·83	99·22	99·21	96·18	100·18	100·07	95·97	99·03	99·50	99·70	95·18	100·41	99·17
O =	22	18	8	8	22	18	8	8	22	18	8	8	22	8	8	22	18	8	8	22	8	8
Si	5·39	4·99	2·10	2·78	5·46	5·05	2·20	2·78	5·45	4·99	2·71	2·74	5·42	2·13	2·65	5·37	5·02	2·13	2·77	5·48	2·19	2·75
Ti	0·53	—	—	—	0·54	—	—	—	0·52	—	—	—	0·05	—	—	0·25	—	—	—	0·40	—	—
Al	3·26	4·04	1·93	1·23	3·28	3·96	1·84	1·24	3·24	4·09	1·31	1·27	3·62	1·87	1·36	3·48	4·01	1·89	1·23	2·99	1·82	1·25
Fe	2·37	0·73	—	—	2·64	0·84	—	—	2·54	0·86	—	—	2·39	—	—	2·55	0·80	—	—	2·32	—	0·03
Mn	—	0·06	—	—	—	0·08	—	—	0·05	—	—	—	—	—	—	0·09	0·04	—	—	0·06	—	—
Mg	1·89	1·10	—	—	1·52	1·04	—	—	1·73	1·04	—	—	2·47	—	—	1·94	1·07	—	—	2·46	—	—
Ca	—	—	0·85	0·20	—	—	0·76	0·18	—	—	0·26	0·24	—	0·86	0·34	—	—	0·83	0·22	—	0·79	0·23
Na	0·26	0·15	0·10	0·79	0·11	—	0·19	0·79	—	—	0·71	0·78	—	0·12	0·65	0·22	0·08	0·15	0·74	—	0·19	0·74
K	1·76	—	0·01	—	1·71	—	—	0·02	1·73	—	0·01	—	1·56	—	0·01	1·71	—	—	0·02	1·84	—	0·01
Total	15·46	11·07	4·99	5·00	15·26	10·97	4·99	5·01	15·26	10·98	5·00	5·03	15·51	4·99	5·01	15·61	11·02	5·00	4·98	15·55	5·00	5·00

(continued)

Downloaded from http://petrology.oxfordjournals.org/ by guest on June 28, 2012

Table 1: Continued

Rock type:	Hb-tonalite (Loc. 1)					Quartz-diorite (Loc. 1)					Quartz-diorite- comb-layer (Loc. 1)					Tokuwa main pluton				
Sample no.:	MGZ-26					MGZ-16c-3					MGZ-16c-1					EZ-01b				
Mineral:	Bt†	Pl-core	Pl-rim	Hb-core†	Hb-rim	Bt†	Pl-core	Pl-rim	Hb-core†	Hb-rim	Bt	Pl-core	Pl-rim	Hb-core	Hb-rim	Bt	Pl-core	Pl-rim	Hb-core	Hb-rim
Oxides (wt %)																				
SiO_2	35·05	48·80	61·56	45·78	46·73	34·16	48·22	55·92	45·87	47·06	35·46	49·36	46·37	46·66	47·41	34·93	45·98	62·95	46·27	48·28
TiO_2	3·83	—	—	1·13	0·74	3·77	—	—	0·97	1·17	3·32	—	—	1·69	0·74	3·13	—	—	1·68	0·58
Al_2O_3	13·69	32·96	24·32	6·06	5·37	14·96	33·53	27·93	7·08	6·66	14·85	32·82	34·19	7·44	5·76	13·19	34·42	23·72	7·31	5·21
FeO(total)	26·97	—	—	21·60	21·77	25·98	—	—	19·57	19·46	24·01	—	0·61	16·87	19·04	25·20	0·38	—	17·69	20·32
MnO	—	—	—	0·31	0·35	—	—	—	0·32	0·30	—	—	—	0·36	0·41	0·49	—	—	—	0·84
MgO	7·64	—	—	9·37	9·13	9·14	—	—	10·37	10·96	9·35	—	—	11·92	11·09	8·59	—	—	11·62	10·85
CaO	0·16	15·96	5·65	10·29	10·21	0·26	16·43	10·06	10·35	10·17	0·45	14·97	17·06	10·54	10·59	—	17·96	4·41	10·50	9·77
Na_2O	0·36	2·39	8·35	1·07	0·51	0·40	2·19	5·70	0·89	0·76	—	2·98	1·45	1·21	0·69	—	1·15	9·08	1·29	0·99
K_2O	7·93	—	0·19	0·55	0·33	6·72	—	—	0·47	0·31	7·75	—	—	0·15	0·18	9·19	—	0·19	0·61	0·47
Total	95·62	100·11	100·07	96·18	95·15	95·40	100·37	99·60	95·89	96·86	95·20	100·14	99·69	96·82	95·91	94·73	99·89	100·36	96·97	97·31
O =	22	8	8	23	23	22	8	8	23	23	22	8	8	23	23	22	8	8	23	23
Si	5·52	2·23	2·73	7·08	7·27	5·34	2·20	2·52	7·03	7·10	5·51	2·25	2·14	6·98	7·22	5·57	2·12	2·77	6·96	7·29
Ti	0·45	—	—	0·13	0·09	0·44	—	—	0·11	0·13	0·39	—	—	0·19	0·08	0·38	—	—	0·19	0·07
Al	2·54	1·77	1·27	1·11	0·98	2·76	1·80	1·48	1·28	1·18	2·72	1·76	1·86	1·31	1·03	2·48	1·87	1·23	1·29	0·93
Fe	3·55	—	—	2·79	2·83	3·39	—	—	2·51	2·46	3·12	—	0·02	2·11	2·42	3·36	0·01	—	2·22	2·57
Mn	—	—	—	0·04	0·05	—	—	—	0·04	0·04	—	—	—	0·05	0·05	0·07	—	—	—	0·11
Mg	1·80	—	—	2·17	2·12	2·13	—	—	2·37	2·47	2·17	—	—	2·66	2·52	2·05	—	—	2·61	2·45
Ca	0·03	0·78	0·27	1·71	1·70	0·04	0·80	0·49	1·70	1·64	0·08	0·73	0·84	1·69	1·73	—	0·89	0·21	1·69	1·58
Na	0·11	0·21	0·72	0·32	0·15	0·12	0·19	0·50	0·26	0·22	—	0·26	0·13	0·35	0·20	—	0·10	0·78	0·38	0·29
K	1·59	—	0·01	0·11	0·07	1·34	—	—	0·09	0·06	1·54	—	—	0·03	0·04	1·87	—	0·01	0·12	0·09
Total	15·60	4·99	5·00	15·45	15·26	15·57	5·00	4·99	15·40	15·31	15·51	5·00	5·00	15·36	15·30	15·75	5·00	5·00	15·45	15·37

*Compositions used for the geothermobarometry.
†Compositions used for the mass-balance calculations.

Downloaded from http://petrology.oxfordjournals.org/ by guest on June 28, 2012

Table 2: Representative whole-rock major element, trace element and Sr-isotope composition, and modal mineralogy of Crd-tonalite, migmatites, hornfels and Tokuwa pluton

Rock type:	Crd-tonalite		Diatexite				Leucosome	Schollen	Metatexite			
Sample no.:	MKG-23c	MKG-33g	MKG-30c	MKG-33f	MG-het-C-1	MKG-33h	MG-het-c-leu	MG-het-c-pf	MKG-30a	MKG-33a	MKG-33i	MKG-33j
Major elements (wt %)												
SiO_2	70·50	70·84	71·24	72·00	70·78	68·06	74·11	54·98	61·39	69·22	65·58	78·21
TiO_2	0·43	0·43	0·66	0·51	0·58	0·74	0·35	1·08	0·89	0·64	0·64	0·39
Al_2O_3	14·88	14·68	14·51	14·58	14·89	15·12	13·85	23·40	20·39	16·34	19·97	12·04
FeO(total)	4·43	4·22	4·73	3·69	4·22	5·57	2·42	6·56	6·19	4·70	4·60	2·82
MnO	0·09	0·08	0·07	0·05	0·06	0·08	0·03	0·12	0·07	0·05	0·07	0·04
MgO	1·62	1·48	1·57	1·23	1·36	1·86	0·78	2·51	1·79	1·23	1·61	0·90
CaO	2·99	2·72	2·13	1·78	1·58	2·63	1·28	3·43	0·74	1·09	1·11	1·42
Na_2O	3·16	3·08	3·03	2·89	2·85	3·21	2·50	5·80	2·24	2·63	2·40	2·57
K_2O	1·88	2·41	2·05	3·24	3·63	2·71	4·62	2·04	6·24	4·08	4·00	1·60
P_2O_5	0·03	0·04	0·01	0·02	0·05	0·03	0·06	0·09	0·06	0·03	0·02	0·01
Total	100·00	100·00	100·00	100·00	100·00	100·00	100·00	100·00	100·00	100·00	100·00	100·00
A.S.I.*	1·17	1·16	1·31	1·27	1·30	1·16	1·21	1·30	1·73	1·52	1·94	1·41
Trace elements (ppm)												
Ba	332·7	430·1	465·7	1000·8	916·8	671·2	1201·4	306·1	760·3	630·0	935·3	276·2
Co	9·8	8·2	11·5	10·4	13·9	14·0	8·1	18·6	15·0	11·2	10·2	6·7
Cr	13·9	14·6	41·9	32·3	37·8	45·4	16·3	68·5	64·0	40·6	40·0	23·5
Cu	4·1	9·4	18·5	20·6	24·7	28·7	9·8	9·6	37·5	38·3	23·8	26·5
Nb	7·7	7·1	12·4	11·8	9·1	10·0	6·4	15·6	18·0	15·5	15·7	11·4
Ni	8·2	3·5	20·4	18·1	20·2	27·0	14·8	18·8	40·9	24·5	23·5	9·0
Rb	117·3	123·5	96·3	110·8	144·5	136·5	144·0	139·7	169·2	120·5	109·5	57·1
Sr	154·2	155·1	172·4	193·7	175·6	184·9	190·6	251·2	111·8	149·2	157·5	139·1
V	92·7	85·2	99·2	72·4	89·4	121·4	49·9	174·9	150·4	93·9	99·8	43·4
Y	25·5	26·1	29·0	32·3	31·8	35·2	31·1	94·2	33·8	27·0	35·8	27·8
Zn	76·1	76·4	91·3	76·7	82·2	93·3	48·1	127·0	126·0	88·6	97·7	63·1
Zr	107·8	108·5	229·5	190·4	221·7	228·2	153·0	237·8	166·1	228·8	191·3	184·5
$^{87}Sr/^{86}Sr$	0·70707	0·70723	0·70942	0·70966	0·70941	0·70817	0·70940	0·70940	0·71190	0·71076	0·71035	0·71032
SrI(12Ma)	0·70669	0·70684	0·70915	0·70938	0·70901	0·70781	0·70903	0·70912	0·71115	0·71036	0·71000	0·71011
Modal proportions (vol. %)												
quartz	45·3	40·2	53·4	45·9	42·6	31·1	33·9	2·2				
plagioclase	30·8	39·0	26·8	28·3	22·5	37·3	13·1	60·2				
K-feldspar	<1	1·0	3·2	7·4	13·9	6·6	37·9	1·7				
biotite	14·6	16·4	10·0	12·0	13·0	22·7	6·5	27·3				
hornblende												
opaque	<1	<1	<1	<1	1·1	<1	1·0	<1				
cordierite	5·7	<1	5·6	4·3	3·7	<1	2·9	8·6				
muscovite	2·2	1·2	<1	1·3	1·9	<1	4·3					
chlorite		<1		<1		<1						
pinite	<1	1·4	<1	<1	1·3	1·0	<1					

(continued)

Downloaded from http://petrology.oxfordjournals.org/ by guest on June 28, 2012

Table 2: Continued

Rock type:	Hornfels					Tokuwa pluton (Magi River section)						
						Hb-tonalite		Bt-tonalite		Quartz-diorite		
Sample no.:	MKG-20c	MKG-31a	CHA-02	SKW-11†	ITS-03†	MGZ-14c	MGZ-26	MGZ-08b	MGZ-08c	MGZ-09b	MGZ-17a	MGZ-16c-1‡
Major elements (wt %)												
SiO_2	70·52	69·90	72·13	67·75	76·51	64·62	62·88	71·97	70·26	58·02	56·29	48·91
TiO_2	0·64	0·68	0·64	0·75	0·44	0·52	0·57	0·47	0·44	0·86	0·80	0·85
Al_2O_3	15·81	15·63	15·39	16·96	13·61	16·60	16·77	14·41	15·43	17·30	17·48	18·07
FeO(total)	5·33	5·70	4·30	5·55	2·69	5·67	6·17	3·72	3·88	8·64	9·37	11·27
MnO	0·05	0·12	0·05	0·24	0·03	0·15	0·15	0·04	0·04	0·19	0·19	0·21
MgO	2·06	2·20	1·95	1·93	0·99	2·15	2·51	0·99	1·00	3·58	4·04	6·19
CaO	0·60	0·59	0·81	1·34	0·50	5·67	6·06	3·58	3·87	7·43	8·22	12·86
Na_2O	1·82	1·68	1·31	1·51	1·92	3·31	4·09	3·62	3·85	2·92	2·79	1·40
K_2O	3·13	3·45	3·37	3·84	3·26	1·23	0·71	1·12	1·22	0·95	0·76	0·22
P_2O_5	0·03	0·04	0·06	0·13	0·05	0·09	0·09	0·07	0·03	0·10	0·07	0·01
Total	100·00	100·00	100·00	100·00	100·00	100·00	100·00	100·00	100·00	100·00	100·00	100·00
A.S.I.*	2·11	2·06	2·11	1·87	1·79	0·97	0·91	1·05	1·05	0·89	0·86	0·70
Trace elements (ppm)												
Ba	505·5	547·5	620·0	703·6	479·0	239·7	128·6	288·5	378·4	156·6	110·2	21·8
Co	14·1	15·4	21·8	19·2	7·7	17·1	18·6	11·4	12·2	25·3	27·9	34·0
Cr	63·3	56·6	61·6	62·7	36·3					3·9	8·9	8·1
Cu	61·8	93·2	158·4	65·7	39·8	4·8		32·1	33·8	23·9	29·0	41·8
Nb	14·3	13·8	10·9	11·6	11·6	2·7	2·6	4·7	4·6	2·8	1·9	0·7
Ni	49·3	48·6	65·6	38·7	19·8			3·8	3·1	2·7	3·5	2·4
Rb	112·6	133·2	120·9	113·8	108·0	40·9	19·1	67·3	70·9	33·1	20·2	3·5
Sr	149·5	147·8	134·2	148·7	93·8	223·8	201·9	174·3	198·4	230·6	210·1	197·5
V	120·4	126·7	127·6	143·2	64·5	126·4	129·1	62·1	64·7	221·5	291·7	472·8
Y	22·5	23·1	24·8	27·5	21·2	23·4	24·3	26·3	26·7	22·2	21·2	13·8
Zn	128·9	126·1	179·6	129·1	40·0	77·4	96·6	60·0	68·2	92·0	82·1	83·8
Zr	137·9	137·6	130·3	153·5	183·5	90·3	71·9	112·6	123·9	57·9	57·9	20·3
$^{87}Sr/^{86}Sr$	0·70976	0·71051	0·71032	0·70891	0·71101	0·70463	0·70403	0·70561	0·70553		0·70445	0·70431
SrI(12Ma)	0·70939	0·71006	0·70995	0·70853	0·71044	0·70454	0·70398	0·70542	0·70536		0·70440	0·70430
Modal proportions (vol. %)												
quartz						28·4	25·4	38·4	34·2	12·2	7·8	<1
plagioclase						56·8	55·3	46·3	54·7	53·8	53·5	48·3
K-feldspar								2·0	<1			
biotite						9·9	3·0	12·5	9·5	12·3	3·3	1·9
hornblende						4·6	15·9			20·3	32·5	47·9
opaque						<1	<1	<1	1·0	1·4	1·2	1·6
cordierite												
muscovite												
chlorite							<1				1·7	
pinite												

(continued)

Downloaded from http://petrology.oxfordjournals.org/ by guest on June 28, 2012

Table 2: Continued

Rock type:	Tokuwa main pluton (external part)						Tokuwa main pluton (internal part)					
Sample no.:	MKG-03	MKG-05b	MKG-08	MGZ-04	EZ-07	YAK-15	HRS-15	YZ-02a	YZ-03	EZ-01b	EZ-12	HIK-08
Major elements (wt %)												
SiO_2	62·95	55·30	68·44	68·29	57·10	67·96	65·48	73·44	66·08	67·11	65·17	64·09
TiO_2	0·57	0·72	0·42	0·42	0·64	0·42	0·51	0·24	0·52	0·45	0·52	0·58
Al_2O_3	16·11	17·87	14·84	15·50	16·10	15·31	15·76	14·01	15·72	15·47	15·61	16·04
FeO(total)	6·52	9·26	4·50	4·40	8·58	4·53	5·39	2·36	5·33	4·88	5·84	6·06
MnO	0·14	0·18	0·11	0·10	0·20	0·10	0·11	0·04	0·10	0·10	0·13	0·13
MgO	3·08	4·62	1·85	1·73	5·10	1·82	2·23	0·93	2·03	1·92	2·35	2·42
CaO	6·31	9·12	3·88	4·02	8·20	4·40	5·32	2·76	4·46	4·44	4·68	5·18
Na_2O	2·51	1·97	2·70	3·04	2·70	2·90	2·69	2·51	2·81	2·81	2·72	2·84
K_2O	1·79	0·97	3·26	2·44	1·35	2·55	2·51	3·72	2·92	2·79	2·97	2·62
P_2O_5	0·02	0·00	0·00	0·06	0·02	0·02	0·01	0·00	0·03	0·02	0·02	0·04
Total	100·00	100·00	100·00	100·00	100·00	100·00	100·00	100·00	100·00	100·00	100·00	100·00
A.S.I.*	0·92	0·86	0·99	1·04	0·77	0·99	0·94	1·06	0·99	0·98	0·96	0·95
Trace elements (ppm)												
Ba	330·8	119·9	529·4	526·0	204·3	371·9	473·7	504·5	518·6	489·6	508·5	499·4
Co	19·3	28·0	14·7	13·9	25·2	14·6	18·8	5·9	17·0	17·1	18·1	19·2
Cr	23·8	16·6	15·4	1·3	37·1	5·5	13·9	0·0	11·3	6·3	12·8	8·2
Cu	10·2	8·8	14·4	7·1	14·2	13·9	25·1	9·9	37·5	22·0	20·3	21·6
Nb	5·2	2·9	5·3	4·6	7·1	5·2	5·6	3·1	5·6	3·7	5·7	5·2
Ni	6·9	9·2	8·0	4·2	6·7	5·4	4·9	1·3	5·1	3·0	6·7	6·5
Rb	63·5	26·2	121·4	71·9	53·4	96·6	84·3	118·0	104·2	109·3	113·2	108·0
Sr	196·0	199·7	145·8	182·6	185·6	160·7	179·7	132·7	175·5	164·6	168·0	178·8
V	181·2	257·8	104·6	103·6	214·0	99·8	125·8	46·5	120·1	121·9	131·4	146·5
Y	23·5	15·8	21·7	20·2	44·0	21·3	27·2	8·9	21·8	20·3	32·0	22·2
Zn	75·3	71·7	54·6	58·3	94·6	57·3	62·2	43·1	57·3	54·9	63·1	63·0
Zr	103·8	36·2	103·3	87·8	85·6	95·6	120·5	88·9	101·5	99·8	116·2	100·9
$^{87}Sr/^{86}Sr$	0·70527	0·70403	0·70538	0·70520	0·70524	0·70530	0·70474	0·70502	0·70487	0·70488	0·70488	0·70502
SrI(12Ma)	0·70511	0·70397	0·70497	0·70500	0·70509	0·70500	0·70452	0·70458	0·70458	0·70456	0·70455	0·70472
Modal proportions (vol. %)												
quartz	25·8	13·7	30·0	30·4	15·4	29·8	26·9	42·1	32·1	28·8	29·0	27·2
plagioclase	49·2	59·2	34·2	45·6	45·8	48·7	50·7	28·7	45·8	44·8	33·2	44·0
K-feldspar	1·9		15·0	9·7	<1	7·2	9·4	24·5	5·5	13·0	15·2	4·1
biotite	13·9	<1	16·2	8·3	6·2	9·8	4·6		7·7	6·1	10·1	16·4
hornblende	8·3	19·4	4·2	5·5	31·1	4·4	7·2		4·6	6·1	9·2	8·2
opaque	<1	2·4	<1	<1	<1	<1	<1	<1	<1	<1	<1	<1
cordierite												
muscovite												
chlorite	<1	4·7		<1	<1		<1	4·6	3·6	1·2	2·3	<1
pinite												

*Alumina saturation index = molar $Al_2O_3/(CaO + Na_2O + K_2O)$.
†Data from Saito *et al.* (2004).
‡Comb-layer.

Downloaded from http://petrology.oxfordjournals.org/ by guest on June 28, 2012

Table 3: Summary of representative mineral assemblages and textures indicative of melt involvement in the rocks of the contact aureole

Sample no.	Rock type	Assemblage	Textures indicative of melt involvement			
			Zoned Pl	An-rich core in Pl	Thin film development	Crystal surface development
Loc. 1						
MGZ-06	Hornfels	Bt + Ms + Chl + Qtz + Pl	x	x	x	x
MKG-31a	Hornfels	Crd + Bt + Ms + Qtz + Pl ± Chl	x	x	x	x
MGZ-11	Hornfels	And + Crd + Bt + Qtz + Pl + Ms ± Chl	x	x	x	x
MGZ-34b	Hornfels	Grt + Crd + Bt + Ms + Qtz + Pl	x	x	x	x
MGZ-47	Hornfels	Kfs + Crd + Bt + Qtz + Pl ± Ms	x	x	x	x
MGZ-46	Hornfels	And + Kfs + Crd + Bt + Ms + Qtz + Pl	x	x	x	x
MGZ-49	Hornfels	Sil + And + Kfs + Crd + Bt + Ms + Pl ± Qtz ± Crn	x	x	x	x
MGZ-17c	Metatexite	Sil + And + Kfs + Crd + Bt + Ms + Pl ± Qtz ± Crn	o	x	o	x
MKG-33d	Metatexite	Kfs + Crd + Bt + Qtz + Pl ± Ms	o	x	o	o
MKG-35a	Diatexite	Kfs + Crd + Bt + Qtz + Pl ± Ms	o	o	o	o
MKG-23c	Crd-tonalite	Crd + Bt + Qtz + Pl ± Ms ± Kfs	o	o	o	o
Loc. 2						
MGZ-03a	Metatexite	Grt + Kfs + Crd + Bt + Qtz + Pl	o	x	o	o
Loc. 3						
HIK-13	Metatexite	Grt + Kfs + Crd + Bt + Qtz + Pl	o	x	o	o
Loc. 4						
SKW-06	Metatexite	Kfs + Bt + Qtz + Pl	o	x	o	o
Loc. 5						
AOZ-11a	Metatexite	Kfs + Crd + Bt + Qtz + Pl	o	x	o	o

MIGMATITES AND ASSOCIATED CORDIERITE-BEARING TONALITE AT LOC. 1-a

Diatexite and cordierite-bearing tonalite occur together with metatexite in a narrow zone along a stream located in the northern part of the Magi River section (Loc. 1-a; Fig. 2b). Although thick soil cover and dense vegetation hamper the observation of a direct contact relationship between the migmatite and the Tokuwa pluton, the rocks at this locality provide an excellent opportunity to examine genetic relationships between the migmatites, cordierite-bearing tonalite, and Tokuwa pluton. The rocks at Loc. 1-a are grouped into three types based on their macroscopic textural characteristics: (1) metatexite containing leucosome; (2) diatexite containing discrete leucosomes and schollen; (3) cordierite-bearing tonalite (Crd-tonalite). There is gradational transition between these rock types (Fig. 7). The metatexite, diatexite, and Crd-tonalite have nearly identical mineral assemblages of quartz + plagioclase + biotite + cordierite ± K-feldspar ± muscovite. Zircon, apatite, monazite, pyrite, spinel, tourmaline, pyrrhotite and ilmenite are accessory minerals.

The migmatite terminology used throughout this study is defined as follows (see Mehnert, 1968; Brown, 1973; Pattison & Harte, 1988; Sawyer, 1996): (1) metatexite: the migmatite that preserves pre-migmatization structures; (2) diatexite: the migmatite in which pre-migmatization structures are completely overprinted; (3) mesosome: the mesocratic part, with decussate and/or granoblastic textures, of the metatexite, which is finer-grained than the leucosome; (4) leucosome: the leucocratic plutonic part, poor in mafic minerals; (5) schollen: the melanocratic fragments within the diatexite.

Metatexite

The metatexite consists of mica-rich pelitic and quartz-rich psammitic layers with quartzofeldspathic leucosomes. The leucosome occurs within pelitic layers or at the interface between pelitic and psammitic layers. The relative proportion of leucosome in the metatexite increases towards the diatexite zone, and finally the rock develops an anastomosing network of leucosomes (Fig. 7b). Cordierite [0·53–0·60 X_{Mg}; $X_{Mg} = Mg/(Mg + Fe)$] in the leucosome occurs as inclusion-free euhedral to subhedral discrete grains (Fig. 5b). In the mesosome it has higher X_{Mg} (0·58–0·62)

Downloaded from http://petrology.oxfordjournals.org/ by guest on June 28, 2012

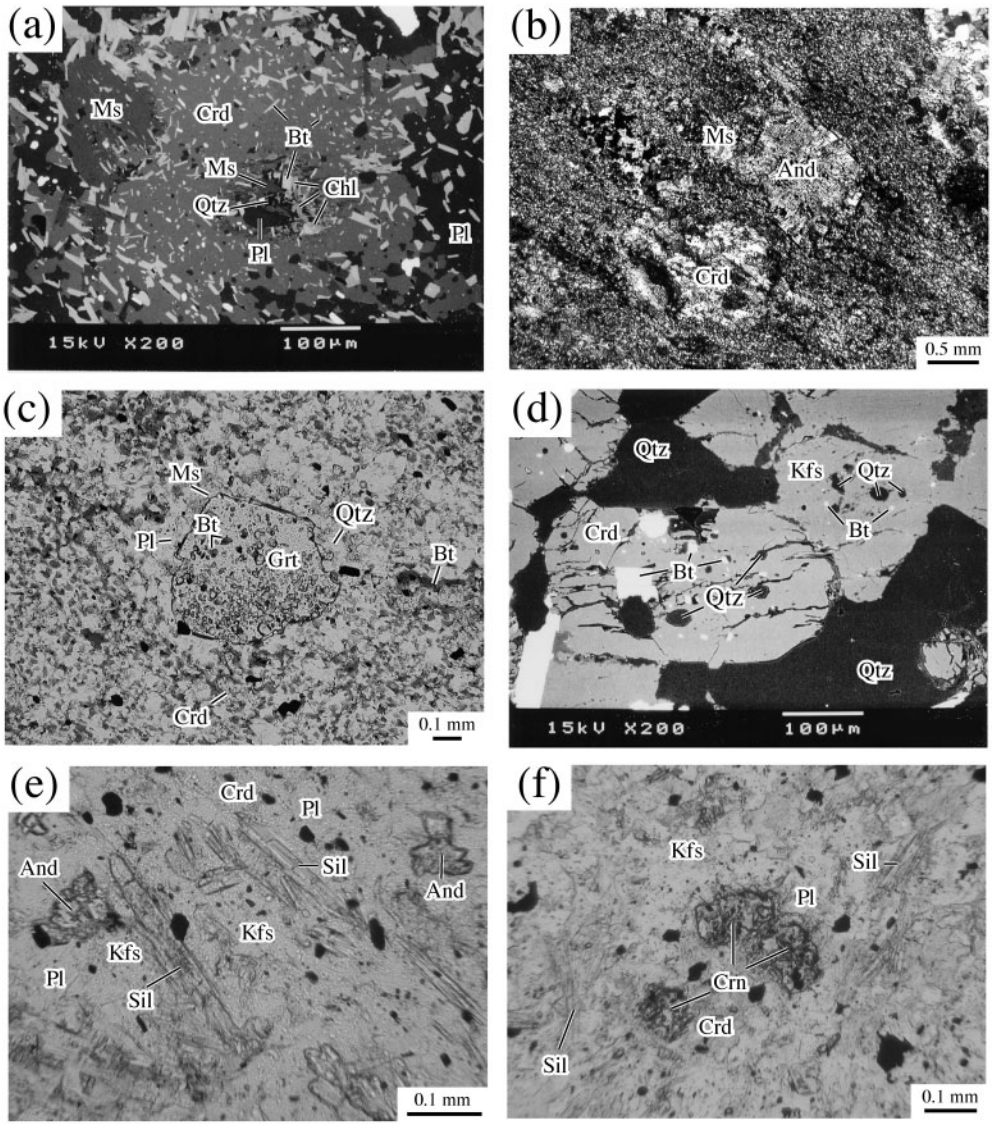


Fig. 4. Representative microstructures in the hornfels from the Tokuwa contact aureole. (a) Poikiloblastic cordierite in the assemblage Crd + Bt + Ms + Qtz + Pl ± Chl. Cordierite contains inclusions of quartz, muscovite, chlorite and biotite. Backscattered electron image. (b) Porphyroblastic andalusite in the assemblage And + Crd + Bt + Ms + Qtz + Pl ± Chl. Cross-polarized light. (c) Poikiloblastic garnet in the assemblage Grt + Crd + Bt + Qtz + Pl + Ms. Garnet contains quartz and biotite inclusions. Plane-polarized light. (d) K-feldspar and cordierite in the assemblage Kfs + Crd + Bt + Qtz + Pl ± Ms. K-feldspar and cordierite contain small grains of Bt and Qtz. Backscattered electron image. (e) Sillimanite and andalusite in the assemblage Sil + And + Kfs + Crd + Bt + Pl + Qtz + Ms. These developed in a matrix of quartz, plagioclase, K-feldspar, and cordierite. Plane-polarized light. (f) Corundum in the assemblage Sil + And + Kfs + Crd + Bt + Pl + Ms. Corundum occurs only in quartz-depleted layers consisting of plagioclase, K-feldspar, cordierite, biotite, muscovite, andalusite and/or sillimanite. Plane-polarized light.

and occurs as poikiloblastic crystals containing inclusions of quartz, plagioclase, muscovite and biotite. Fine-grained (<0·1 mm) hercynitic spinel inclusions occur locally in poikiloblastic cordierite. Plagioclase in both the leucosome and the mesosome exhibits normal chemical zoning. Biotite in the leucosome forms euhedral to subhedral grains and is relatively Fe-rich (0·38–0·41 X_{Mg}) compared with the subhedral to anhedral biotite grains in the mesosome (0·49–0·52 X_{Mg}). K-feldspar in the mesosome contains fine-grained quartz and biotite inclusions.

Diatexite

The diatexite is a medium- to fine-grained rock, containing leucosomes (up to 5 cm long) and schollen (up to 15 cm long). This rock lacks the layered appearance of the metatexite, implying that it has undergone

Downloaded from http://petrology.oxfordjournals.org/ by guest on June 28, 2012

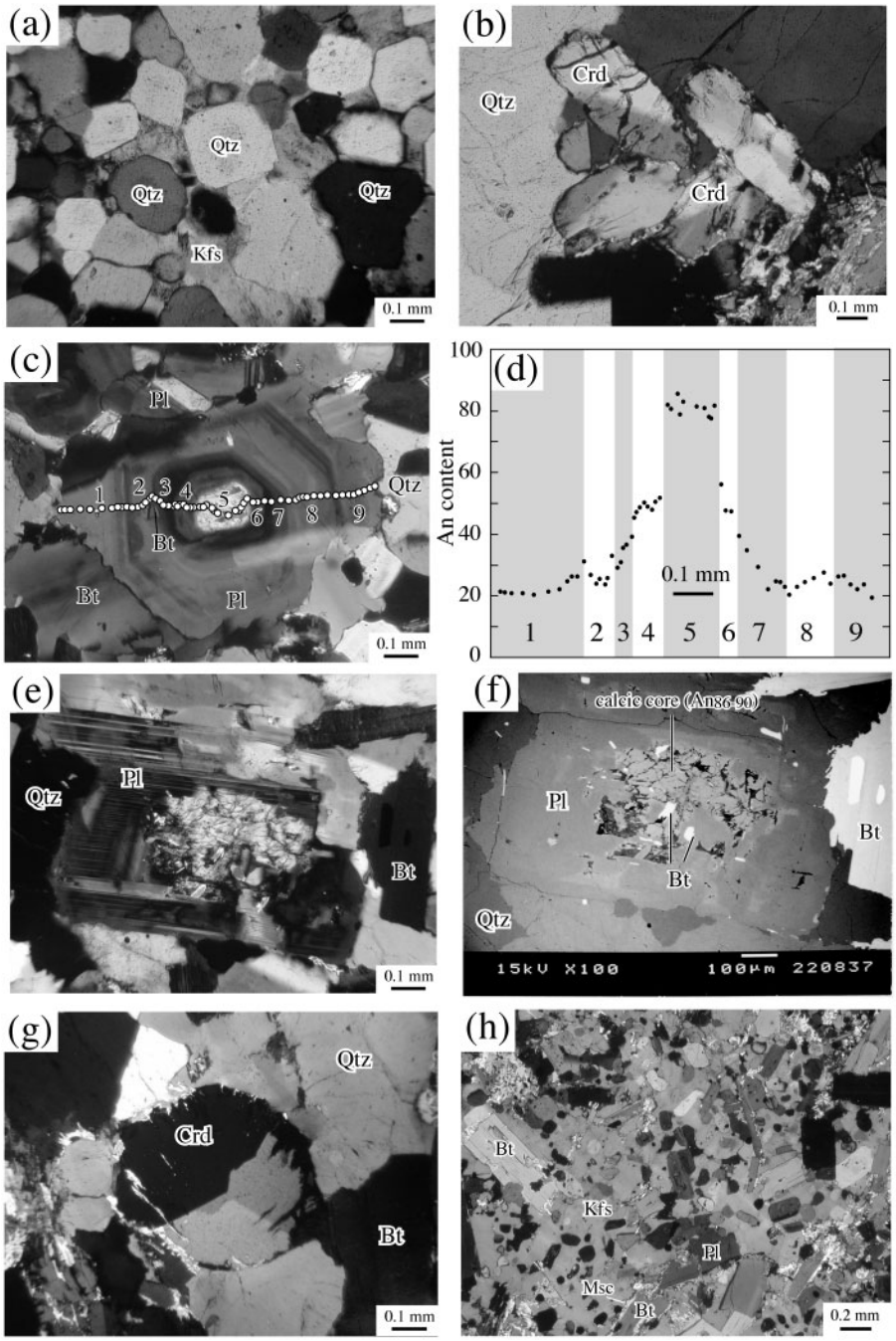


Fig. 5. Representative microstructures of metatexite, diatexite and Crd-tonalite. (a) Leucosome in the migmatite at Loc. 2. K-feldspar contains idioblastic quartz crystals. Cross-polarized light. (b) Inclusion-free cordierite in leucosome of the metatexite at Loc. 1-a. Cross-polarized light. (c) Chemically zoned plagioclase in the diatexite. Small white dots indicate analyzed points. Cross-polarized light. (d) Microprobe profile across the plagioclase shown in (c). (Note highly An-rich core.) (e) Plagioclase in diatexite which contains biotite. (Note irregular-shaped An-rich core.) Cross-polarized light. (f) Backscattered electron image of the plagioclase shown in (e). (Note An-rich core.) (g) Inclusion-free cordierite in the diatexite. Cross-polarized light. (h) Poikilitic K-feldspar in diatexite. K-feldspar contains euhedral to subhedral biotite and rounded plagioclase. Cross-polarized light. (i) Subhedral to euhedral biotite in leucosome within diatexite. Plane-polarized light. (j) Granoblastic texture of schollen in diatexite. Plane-polarized light. (k) Spongy-shaped biotite (outlined by white-dotted line) and strongly zoned plagioclase in biotite-enriched clot incorporated in diatexite. Cross-polarized light. (l) Backscattered electron image of the biotite and plagioclase shown in (k). Small white dots indicate analyzed points. (Note the An-rich core in plagioclase.) (m) Rim of the biotite-rich clot in diatexite. Cordierite-rich part (right) surrounds biotite-rich clot (left). Plane-polarized light. (n) Equigranular texture of the Crd-tonalite. Cross-polarized light.

Downloaded from http://petrology.oxfordjournals.org/ by guest on June 28, 2012

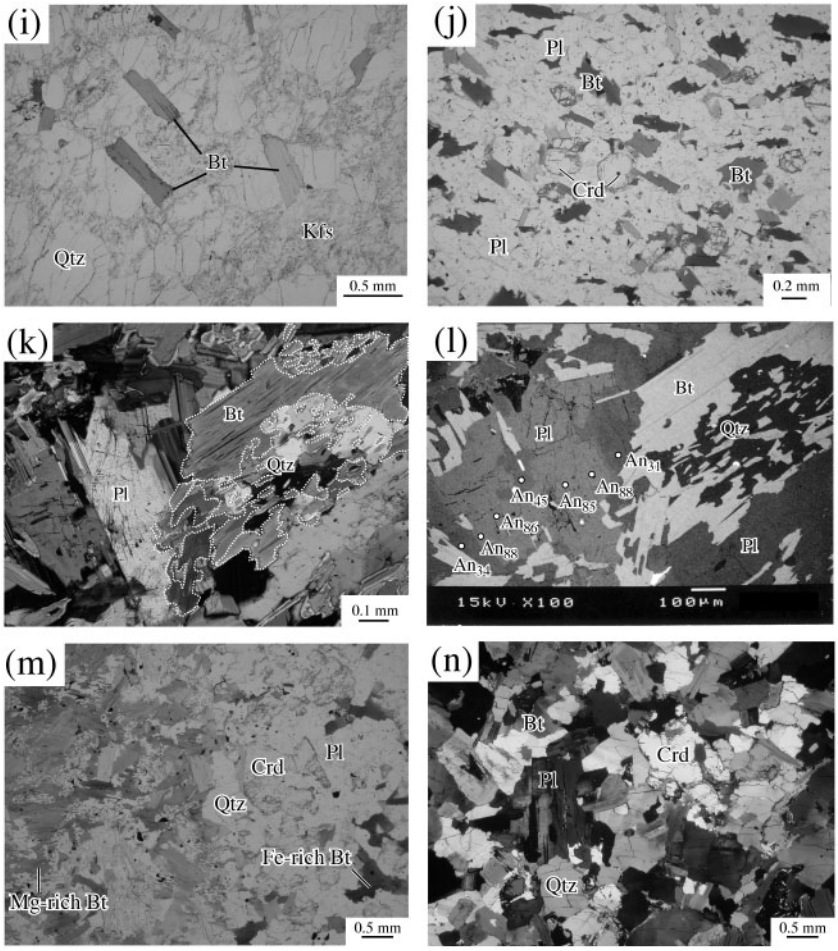


Fig. 5. Continued.

extensive structural homogenization, which overprinted the original sedimentary structures (see Brown, 1973; Bea, 1991; Sawyer, 1996). However, it still has an heterogeneous appearance, comprising a fine-grained migmatitic part with a granoblastic texture and a coarser-grained part with an equigranular and/or poikilitic texture. The rock exhibits a gradational change in grain size and texture (Fig. 7c). Towards the Crd-tonalite zone, the diatexite changes from a fine-grained rock (~0·5 mm grain size) with a granoblastic texture to a medium-grained rock (~1 mm grain size) with an equigranular or poikilitic texture. In a Qtz–Kfs–Pl diagram (Fig. 3), the diatexites straddle the boundary between the granodiorite and granite fields. The mineral assemblage of the diatexite is quartz (31–49 modal %) + plagioclase (23–37 modal %) + K-feldspar (3–19 modal %) + biotite (7–13 modal %) + cordierite (1–10 modal %) ± muscovite (<2 modal %). The diatexite contains chemically zoned plagioclase. The plagioclase has a rounded-shape or sieve-structured calcic core ($An_{75–88}$) mantled by an overgrowth with oscillatory or normal zoning ($An_{19–58}$) (Fig. 5d and f). Fine-grained biotite inclusions occur in the plagioclase (Fig. 5e and f). These biotite inclusions have a wide range of compositions (0·24–0·55 X_{Mg}). Cordierite (0·51–0·63 X_{Mg}) occurs as discrete subhedral to euhedral crystals and has two forms; one is inclusion-free (Fig. 5g) and the other contains small amounts of quartz, biotite and/or muscovite inclusions. In rare cases, cordierite contains fine hercynitic spinel grains (<0·05 mm). The diatexite lacks poikiloblastic cordierite, which is common in the hornfels and metatexite. Biotite in the diatexite matrix occurs predominantly as subhedral to anhedral crystals (0·38–0·45 X_{Mg}). Euhedral to subhedral biotite (0·41–0·45 X_{Mg}), round-shaped plagioclase ($An_{21–28}$), round-shaped quartz, and inclusion-free cordierite (0·55–0·63 X_{Mg}) occur as inclusions in coarse (~10 mm) poikilitic K-feldspar crystals (Fig. 5h).

The leucosomes in the diatexite are coarse-grained (1–2 mm grain size) consisting of K-feldspar (18–40 modal %), quartz (34–41 modal %), plagioclase (13–25 modal %), euhedral to anhedral biotite (7–10 modal %;

Downloaded from http://petrology.oxfordjournals.org/ by guest on June 28, 2012

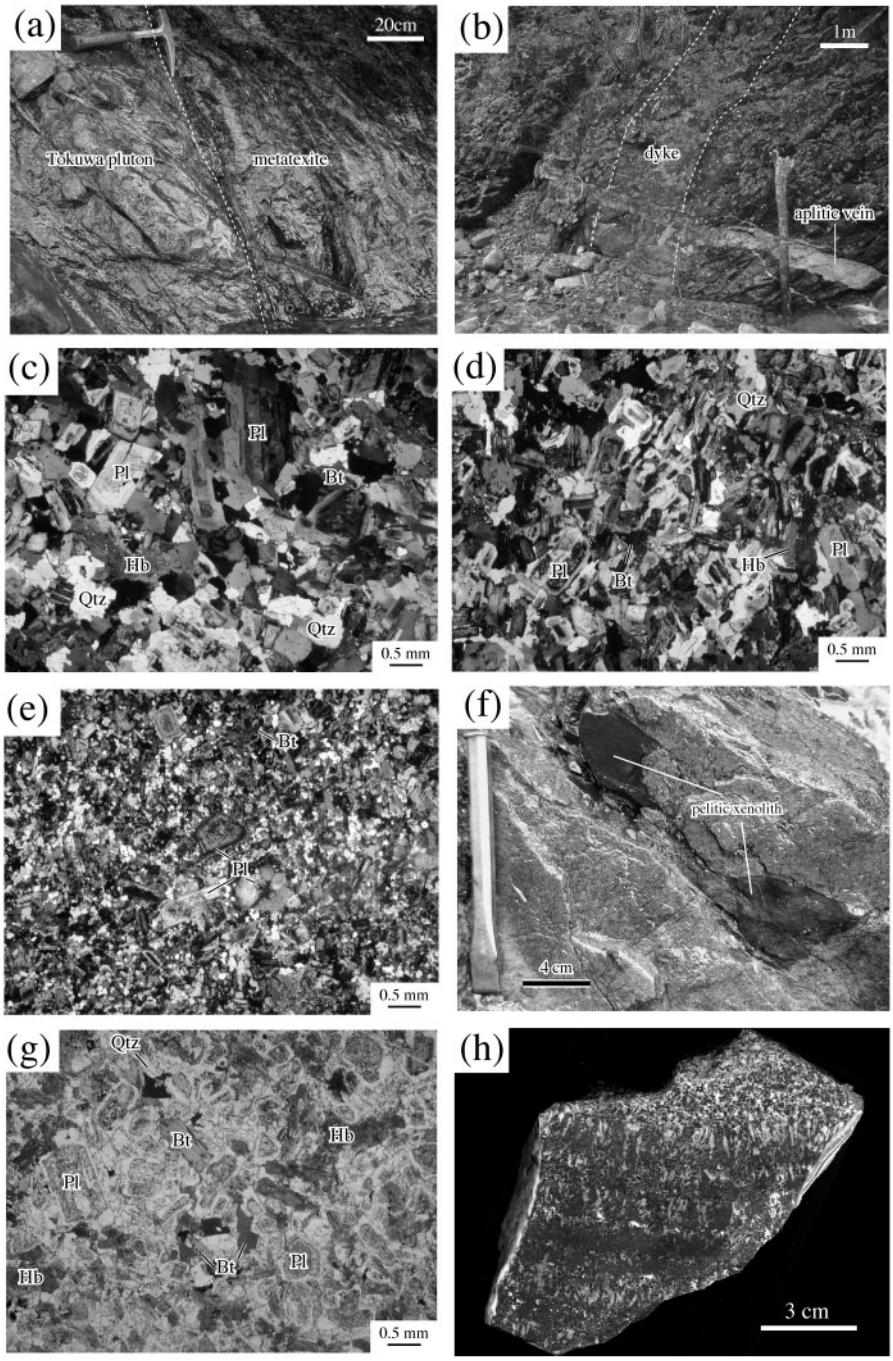


Fig. 6. Field occurrences and representative microstructures of the granitoids in the Magi River section (a) Sharp contact relation between the Tokuwa pluton and host metatexite. (b) Granitoid dykes and aplitic veins in the aureole. (c) Equigranular texture of medium-grained Hb-tonalite at Loc. 1-c. Cross-polarized light. (d) Preferred orientation of subhedral plagioclase in fine-grained Hb-tonalite. Cross-polarized light. (e) Porphyritic texture of Bt-tonalite. Cross-polarized light. (f) Pelitic xenoliths in Bt-tonalite. (g) Cumulate texture of quartz-diorite. Plane-polarized light. (h) Comb-layering structure in quartz-diorite. (Note the plagioclase oriented perpendicular to layers.)

0·33–0·41 X_{Mg}) (Fig. 5i), inclusion-free cordierite (1–3 modal %; 0·51–0·56 X_{Mg}), and muscovite (2–4 modal %). The leucosome falls in the granite field in the modal Qtz–Kfs–Pl diagram (Fig. 3). Plagioclase in the leucosome has either a rounded-shape or a sieve-structured calcic core ($An_{65–80}$) that is mantled by a chemically zoned overgrowth ($An_{18–60}$). In most cases, the leucosomes are developed around schollen. The schollen exhibit a

Downloaded from http://petrology.oxfordjournals.org/ by guest on June 28, 2012

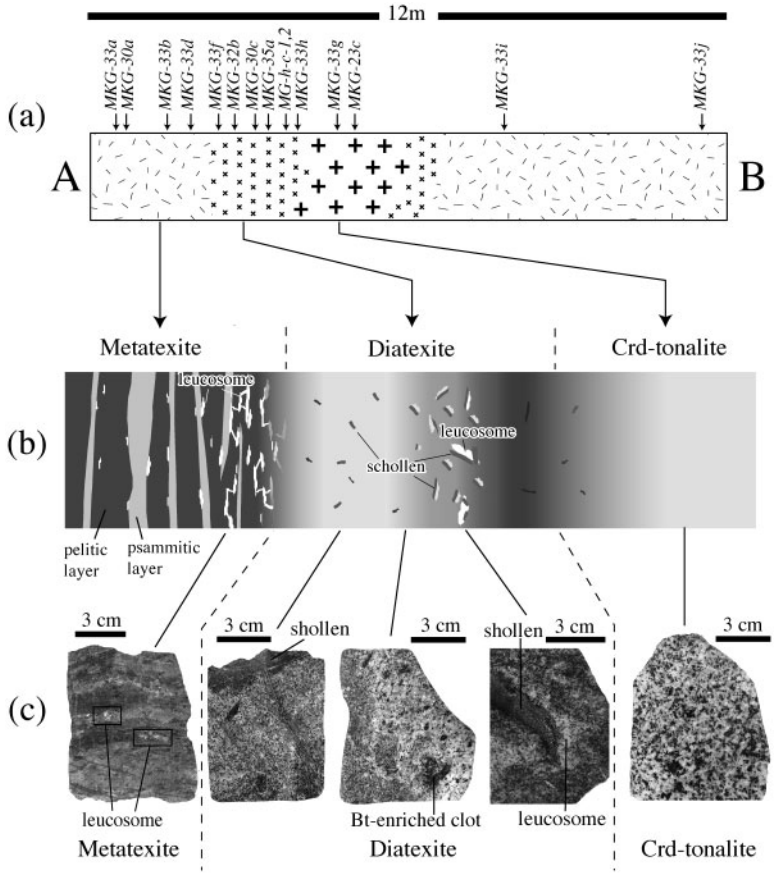


Fig. 7. (a) Sketch map showing field relationships between Crd-tonalite, diatexite and metatexite in the outcrop at Loc. 1-a. Sampling locations for whole-rock chemical analysis are indicated. (b) Schematic illustration showing transitional relationship of Crd-tonalite, diatexite and metatexite. (c) The macroscopic features of migmatites at Loc. 1-a.

granoblastic texture (<0·2 mm grain size) and consist mainly of plagioclase (~60 modal %; $An_{20–26}$), biotite (~27 modal %; 0·35–0·40 X_{Mg}) and cordierite (~9 modal %; 0·54–0·58 X_{Mg}) (Fig. 5j). Biotite in the schollen is subhedral to anhedral and shows a preferred orientation. Fine-grained inclusions of hercynitic spinel (<0·05 mm) are locally observed in the cordierite grains.

Discrete clots (~2 mm long) enriched in biotite occur in the diatexite (Figs 5k, l, m and 7c). These consist of high-Mg and low-Ti biotite (0·51–0·52 X_{Mg}; <0·4 wt % TiO_2), zoned plagioclase ($An_{31–88}$), quartz, and opaque minerals (Fig. 5k and l). The high-Mg and low-Ti biotite has a sponge-like texture (Fig. 5k and l). The clot is surrounded by cordierite-rich regions consisting of inclusion-free cordierite (0·57–0·62 X_{Mg}), zoned plagioclase ($An_{19–90}$), euhedral to anhedral biotite (0·41–0·46 X_{Mg}; 2·4–5·2 wt % TiO_2), and quartz (Fig. 5m).

Cordierite-bearing tonalite

The Crd-tonalite is a homogeneous, medium- to coarse-grained rock (~2 mm grain size) with an equigranular texture (Fig. 5n). It consists mainly of quartz (40–45 modal %), plagioclase (31–39 modal %), biotite (15–16 modal %), cordierite (<6 modal %), muscovite (<2 modal %), and K-feldspar (<1 modal %). In the Qtz–Kfs–Pl diagram, it overlaps the field for tonalite (Fig. 3). As with the diatexite, there are two types of plagioclase in the Crd-tonalite. One has a calcic core ($An_{80–95}$) mantled by an oscillatory or normally zoned ($An_{20–80}$) plagioclase overgrowth and the other exhibits normal compositional zoning ($An_{20–30}$) and lacks a calcic core. The plagioclase with calcic cores contains fine-grained biotite inclusions. Cordierite (0·56–0·60 X_{Mg}) occurs as subhedral grain. In places it contains biotite and/or muscovite inclusions. Biotite (0·39–0·44 X_{Mg}) occurs as subhedral to anhedral crystals.

P–T CONDITIONS AT THE EMPLACEMENT LEVEL OF THE TOKUWA PLUTON

Metamorphic *P–T* conditions were calculated for the garnet-bearing rocks in the contact aureole (Loc. 1-b,

Downloaded from http://petrology.oxfordjournals.org/ by guest on June 28, 2012

Loc. 2 and Loc. 3, Fig. 2). The rock from Loc. 1-b is a hornfels consisting of Grt + Crd + Bt + Qtz + Pl + Ms (Fig. 4c). The rocks from Loc. 2 and Loc. 3 are metatexites with the assemblage Grt + Kfs + Crd + Bt + Qtz + Pl. The mesosome of the migmatites at Loc. 2 and Loc. 3 shows a decussate and granoblastic texture, respectively.

We used the TWQ/202 variant of the TEEWQ thermobarometer of Berman (1991) for the P–T estimation. Solid solution models employed in the calculations are those given by Berman & Aranovich (1996) for garnet and cordierite, by Chatterjee & Froese (1975) for muscovite, and by R. D. Berman & L. Ya. Aranovich (unpublished data, 1997) for biotite. The observed mineral assemblages were used. The calculations were performed in the KFMASH system including almandine, pyrope, annite, phlogopite, Mg-cordierite, quartz, muscovite and H_2O for a rock from Loc. 1-b, and almandine, pyrope, annite, phlogopite, Mg-cordierite, K-feldspar, quartz and H_2O for rocks from Loc. 2 and Loc. 3. The compositions of garnet, biotite, cordierite and muscovite used in the calculations are given in Table 1. The compositions of the rims of the grains were used in the calculation.

The two independent sets of reactions intersect at 597°C and 3·0 kbar for Loc. 1-b, at 660°C and 3·1 kbar for Loc. 2, and at 705°C and 3·1 kbar for Loc. 3 (Fig. 8). The estimated pressure conditions are very close for all the three locations and can therefore be taken to represent the pressure at the emplacement level of the Tokuwa pluton (~10 km depth).

The estimated P–T conditions are shown (Fig. 9) in the KFMASH petrogenetic grid of Pattison & Harte (1997). Two isopleths of Mg/(Mg + Fe) in cordierite (0·55 and 0·65) are shown because the average X_{Mg}(Crd) at Loc. 1-a ranges from 0·55 to 0·65. High activity of water conditions might be caused by the migration of exsolved volatiles from the crystallizing Tokuwa magma into the thermal aureole, or of internal water provided by dehydration reactions of the sedimentary protolith in the aureole, as indicated by the abundance of quartz veins within the hornfels. The P–T conditions estimated by the TWQ calculation for the hornfels at Loc. 1-b are subsolidus, but those calculated for the metatexites at Loc. 2 and 3 occur in the supra-solidus field defined by the H_2O-saturated solidus curve of quartzofeldspathic rocks (Pl + Kfs + Qtz + H_2O = L) (Johannes & Holtz, 1996), consistent with the petrographic observations.

Temperature is estimated for the migmatite in Loc. 3 by employing the Grt–Bt thermometer (TWQ/202, Berman, 1991), in which the compositions of the central part of the garnet and the biotite in the matrix are used (Table 1). The temperature estimated by using the

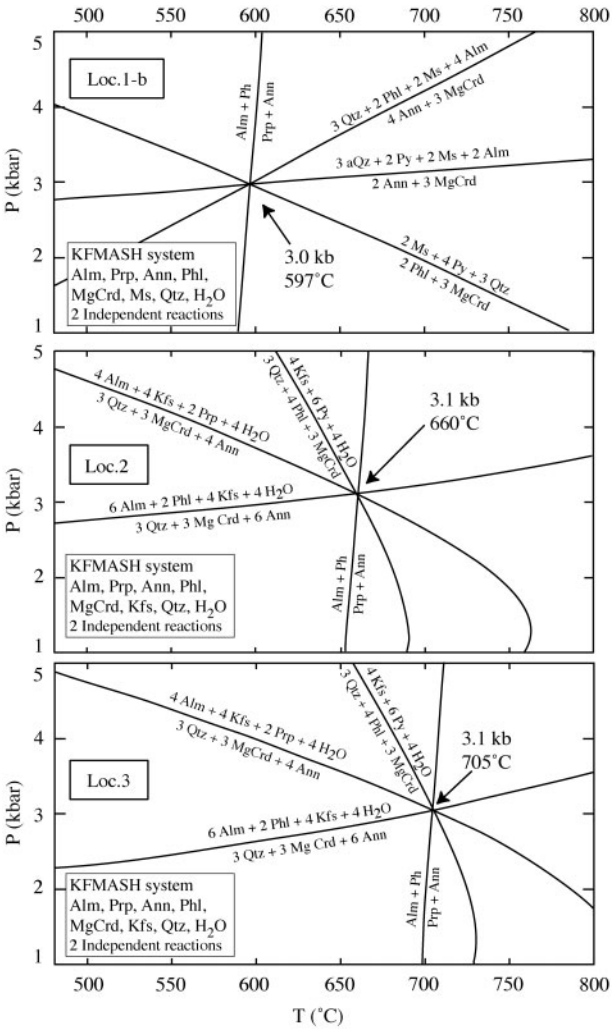


Fig. 8. P–T conditions calculated using TWQ/202 of TEEWQ (Berman, 1991) for garnet-bearing hornfels and migmatite. The estimated pressure conditions are comparable in all three locations and can be considered as the emplacement level (~10 km) of the Tokuwa pluton.

core composition of garnet is 777°C at 3 kbar (Fig. 9), significantly higher than the temperature (705°C) estimated by using the rim compositions of garnet in the same rock sample (Fig. 8). The estimated P–T (~780°C and ~3 kbar) are interpreted as the peak metamorphic conditions, which are located in the supra-solidus field in the Qtz–Ab–Or–H_2O system under relatively high water activity [$a(H_2O) > 0·5$, Fig. 9]. Therefore, we consider that the temperatures estimated by the multi-equilibrium calculations using the garnet rim compositions (Fig. 8) represent minimum temperatures reflecting some degree of Fe–Mg exchange after the thermal peak.

Downloaded from http://petrology.oxfordjournals.org/ by guest on June 28, 2012

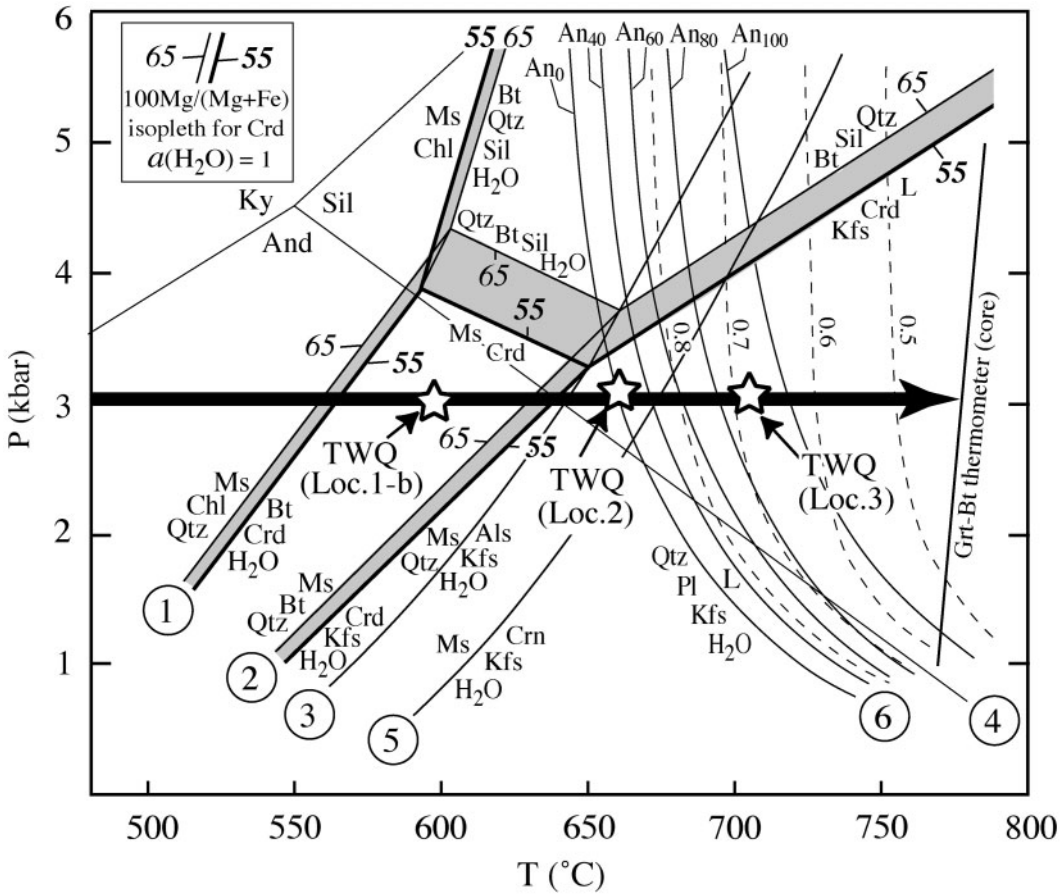


Fig. 9. *P–T* grid of reactions in the KFMASH system at $a(H_2O) = 1$ and $X_{Mg}(Crd) = 0{\cdot}55$–$0{\cdot}65$ (modified after Pattison & Harte, 1997). The *P–T* conditions estimated for garnet-bearing hornfels and migmatites by TWQ (Fig. 8) are also shown (stars). The result of the Grt–Bt thermometer (TWQ/202, Berman, 1991) using the core composition of garnet in the migmatite at Loc. 3 is indicated. Arrow indicates the isobaric heating path at 3 kbar. The reaction Qtz + Pl + Kfs + H_2O = L for different plagioclase compositions is indicated by continuous lines with An content in plagioclase, and the same reaction under various $a(H_2O) = 0{\cdot}8$, 0·7, 0·6 and 0·5 by dashed lines (after Johannes & Holtz, 1996). And = Sil curve is after Pattison (1992).

MICROSTRUCTURES AND INFERRED REACTIONS

Microstructures in hornfels

The Crd-bearing hornfels consists of Crd + Bt + Ms + Qtz + Pl ± Chl. The cordierite occurs as inclusion-rich poikiloblastic crystals containing quartz, chlorite, muscovite and biotite (Fig. 4a), suggesting the cordierite-forming reaction

$$Qtz + Chl + Ms = Crd + Bt + H_2O. \quad (1)$$

The Kfs-bearing hornfels comprises the assemblage Kfs + Crd + Bt + Qtz + Pl ± Ms, where K-feldspar contains inclusions of Bt + Qtz + Pl ± Ms (Fig. 4d). The cordierite has inclusions of Bt + Qtz + Pl (Fig. 4d), suggesting a K-feldspar + cordierite-forming reaction:

$$Qtz + Bt + Ms = Crd + Kfs + H_2O. \quad (2)$$

The Sil-bearing hornfels is characterized by the assemblage Sil + And + Kfs + Crd + Bt + Ms + Qtz + Pl, where sillimanite and andalusite occur in a matrix consisting of Kfs + Crd + Bt + Pl ± Qtz ± Ms (Fig. 4e). These textures suggest an aluminosilicate-forming muscovite–consuming reaction

$$Qtz + Ms = Als + Kfs + H_2O. \quad (3)$$

coinciding with the aluminosilicate-transition reaction

$$And = Sil. \quad (4)$$

In the Crn-bearing hornfels, which has the assemblage Crn + Sil + Kfs + Crd + Bt + Ms + Pl ± Qtz, corundum occurs in the matrix composed of Kfs + Crd + Bt + Pl ± Ms (Fig. 4f). Some corundum is spatially associated with K-feldspar. The textures suggest the corundum-forming reaction

$$Ms = Crn + Kfs + H_2O. \quad (5)$$

Downloaded from http://petrology.oxfordjournals.org/ by guest on June 28, 2012

Microstructures in the metatexite

At Loc. 2, the leucosome in the metatexite consists of quartz and feldspar in which the quartz develops crystal faces against the K-feldspar (Fig. 5a). The absence of euhedral ferromagnesian minerals within the leucosome suggests the following congruent melting reaction:

$$\mathrm{Kfs} + \mathrm{Qtz} + \mathrm{Pl} + \mathrm{H_2O} = \mathrm{L}. \quad (6)$$

The P–T conditions estimated by the TWQ method at Loc. 2 are located on the higher P–T side of reaction (6) (at $\sim \mathrm{An}_0$) in Fig. 9. We suggest that reaction (6) represents the onset of incipient partial melting in the Tokuwa contact aureole.

At Loc. 1-a, the leucosomes in the metatexite consists predominantly of K-feldspar, quartz and inclusion-free cordierite ($\sim$0·55 X_{Mg}) and subordinate subhedral to euhedral biotite, zoned plagioclase, and muscovite. The occurrence of inclusion-free cordierite and euhedral biotite in the leucosome suggests that these minerals are peritectic products of a mica-breakdown melting reaction. The biotite in the mesosome is rich in Mg ($\sim$0·50 X_{Mg}) compared with that in the leucosome ($\sim$0·40 X_{Mg}), suggesting the following melting reaction:

$$\begin{aligned}\mathrm{Qtz} + \mathrm{Ms} + \text{Mg-rich Bt}(\sim 0\cdot 50\ X_{\mathrm{Mg}}) \\ = \mathrm{Crd}(\sim 0\cdot 55\ X_{\mathrm{Mg}}) \\ + \text{Fe-rich Bt}\,(\sim 0\cdot 40\ X_{\mathrm{Mg}}) + \mathrm{L}. \quad (7)\end{aligned}$$

The cordierite-forming peritectic reaction $\mathrm{Sil} + \mathrm{Bt} + \mathrm{Qtz} = \mathrm{Kfs} + \mathrm{Crd} + \mathrm{L}$ is improbable because of the absence of sillimanite at Loc. 1-a. The possibility that the sillimanite was produced, then subsequently consumed by two consecutive prograde reactions ($\mathrm{Ms} + \mathrm{Crd} = \mathrm{Bt} + \mathrm{Sil} + \mathrm{Qtz} + \mathrm{H_2O}$ and $\mathrm{Sil} + \mathrm{Bt} + \mathrm{Qtz} = \mathrm{Kfs} + \mathrm{Crd} + \mathrm{L}$; see Fig. 9) is not likely given that the estimated pressure condition ($\sim$3 kbar) is lower than that for these reactions in the P–T field (Fig. 9).

Microstructures in the diatexite

The Mg-rich biotite (0·47–0·50 X_{Mg}) in the biotite-enriched clots shows a sponge-like texture that is considered to be a breakdown reaction product of Mg-rich biotite involving melt (Fig. 5k and l; see Holtz & Johannes, 1991). The clot is surrounded by cordierite-rich regions consisting of inclusion-free cordierite ($\sim$0·60 X_{Mg}), plagioclase (An_{19-90}), quartz, and Fe-rich biotite (0·39–0·41 X_{Mg}) (Fig. 5m). These petrographic features suggest the following melting reaction:

$$\begin{aligned}\mathrm{Qtz} + \mathrm{Ms} + \text{Na-rich Pl} + \text{Mg-rich Bt}\,(\sim 0\cdot 50\ X_{\mathrm{Mg}}) \\ = \text{Ca-rich Pl}\,(\sim \mathrm{An}_{90}) \\ + \text{Fe-rich Bt}\,(\sim 0\cdot 40\ X_{\mathrm{Mg}}) \\ + \mathrm{Crd}\,(\sim 0\cdot 60\ X_{\mathrm{Mg}}) + \mathrm{L}. \quad (8)\end{aligned}$$

In the system Qtz–Ab–Or–An–H_2O, the reaction $\mathrm{Pl} + \mathrm{Kfs} + \mathrm{Qtz} + \mathrm{H_2O} = \mathrm{L}$ (i.e. the solidus) moves toward higher temperatures with increasing An content in plagioclase (Johannes & Holtz, 1996) (Fig. 9). The plagioclase in the diatexite has irregular-shaped cores with extremely high anorthite contents (An_{80-95}). The P–T conditions ($\sim$780°C and $\sim$3 kbar) estimated using TWQ202 (Berman, 1991) for the aureole plot in the supra-solidus field above the solidus reaction Qtz–Ab–Or–An_{100}–H_2O (Johannes & Holtz, 1996) (Fig. 9). This supports the conclusion that the peak metamorphic conditions in the aureole reached supra-solidus conditions and led to anatexis (Fig. 9)

GEOCHEMISTRY

Major and trace element data and Sr-isotope compositions

Selected major and trace element data and alumina saturation index (A.S.I.) values are plotted against SiO_2 for the Tokuwa pluton samples (Fig. 10a) and for the hornfels, migmatites and Crd-tonalite (Fig. 10b). The initial $^{87}Sr/^{86}Sr$ (SrI) of these rocks is indicated in Fig. 10c.

Tokuwa main pluton

Samples from the Tokuwa main pluton (Fig. 2a) contain 55–73 wt % SiO_2. The Al_2O_3, $FeO_{(total)} + MgO$ and CaO contents are negatively correlated with SiO_2, whereas the Na_2O, K_2O, and Ba contents exhibit a positive correlation. The rocks in the Tokuwa main pluton have metaluminous to slightly peraluminous compositions (A.S.I. = 0·77–1·08) and belong to the 'I-type' granitoid affinity defined by Chappell & White (1974). The A.S.I. values show a positive correlation with SiO_2 (Fig. 10a). In the Ab–An–Or diagram (Fig. 11), most of the samples of the Tokuwa main pluton fall in the granodiorite field, with a few samples (mafic samples, 55–57 wt % SiO_2) plotting in the tonalite field. Most of the mafic samples are rich in poikilitic hornblende, suggestive of a cumulate origin. The SrI of the Tokuwa main pluton ranges from 0·7040 to 0·7051. The lowest SrI (0·7040) sample of the Tokuwa main pluton (MKG-05b, 55 wt % SiO_2) was collected 1 km NNE of the Loc. 1-a.

Marginal rocks of the Tokuwa pluton in the Magi River section

The SiO_2 contents of rocks in the marginal part of Tokuwa pluton in the Magi River section (Fig. 2b) range from mafic (quartz-diorite, 49–56 wt %) through intermediate (Hb-tonalite, 61–65 wt %) to felsic (Bt-tonalite, 70–72 wt %). The samples plot in the tonalite field on the An–Ab–Or diagram and show chemical characteristics that are clearly distinct from those of the rocks of the Tokuwa main pluton (Fig. 11). The major and

Downloaded from http://petrology.oxfordjournals.org/ by guest on June 28, 2012

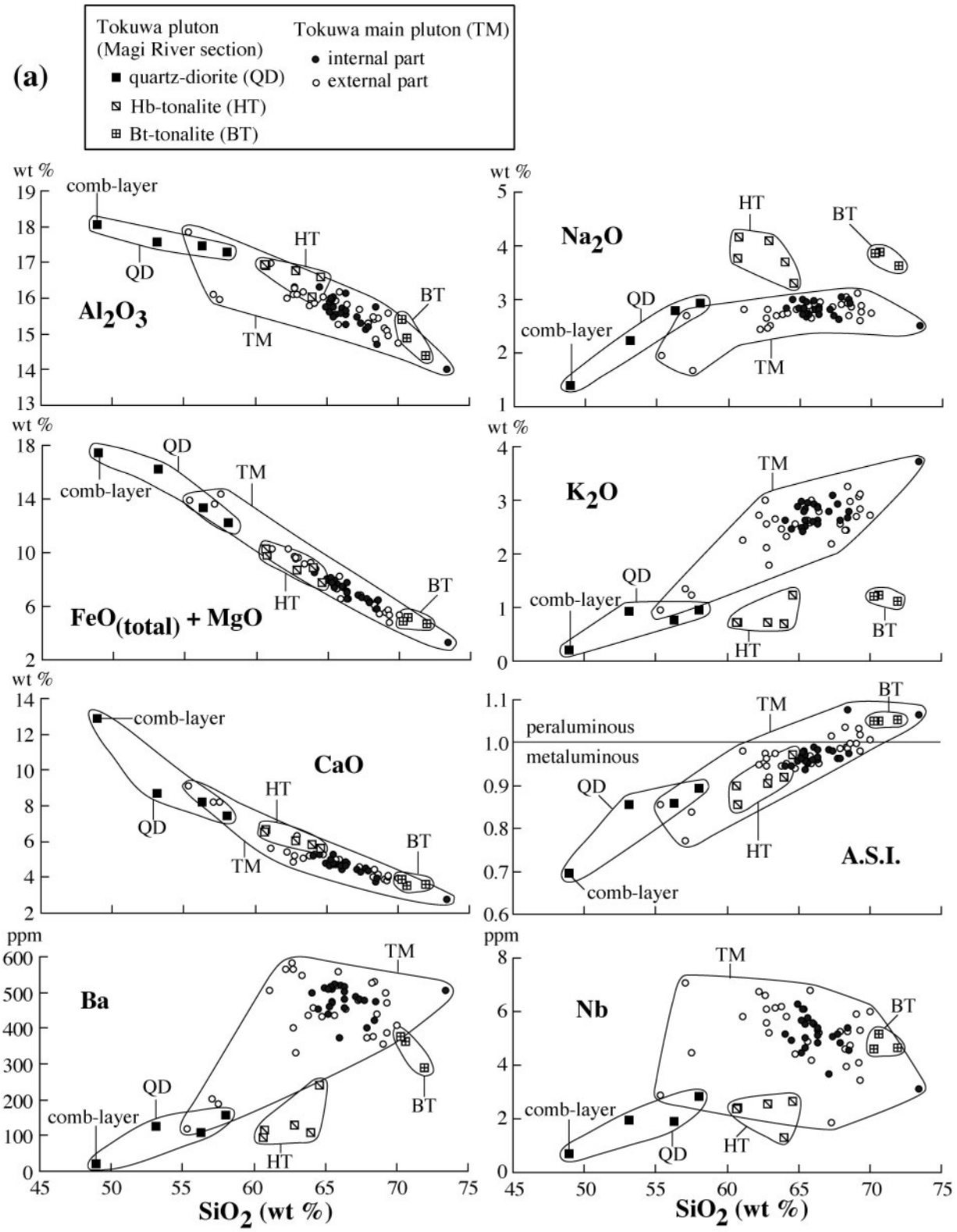


Fig. 10. (a) Major and trace element variation diagrams for granitoids in the Tokuwa pluton. (b) Major and trace element variation diagrams for the Crd-tonalite, diatexite, metatexite and hornfels. (c) SiO_2–SrI diagram for the Tokuwa pluton, Crd-tonalite, diatexite, metatexite and hornfels.

Downloaded from http://petrology.oxfordjournals.org/ by guest on June 28, 2012

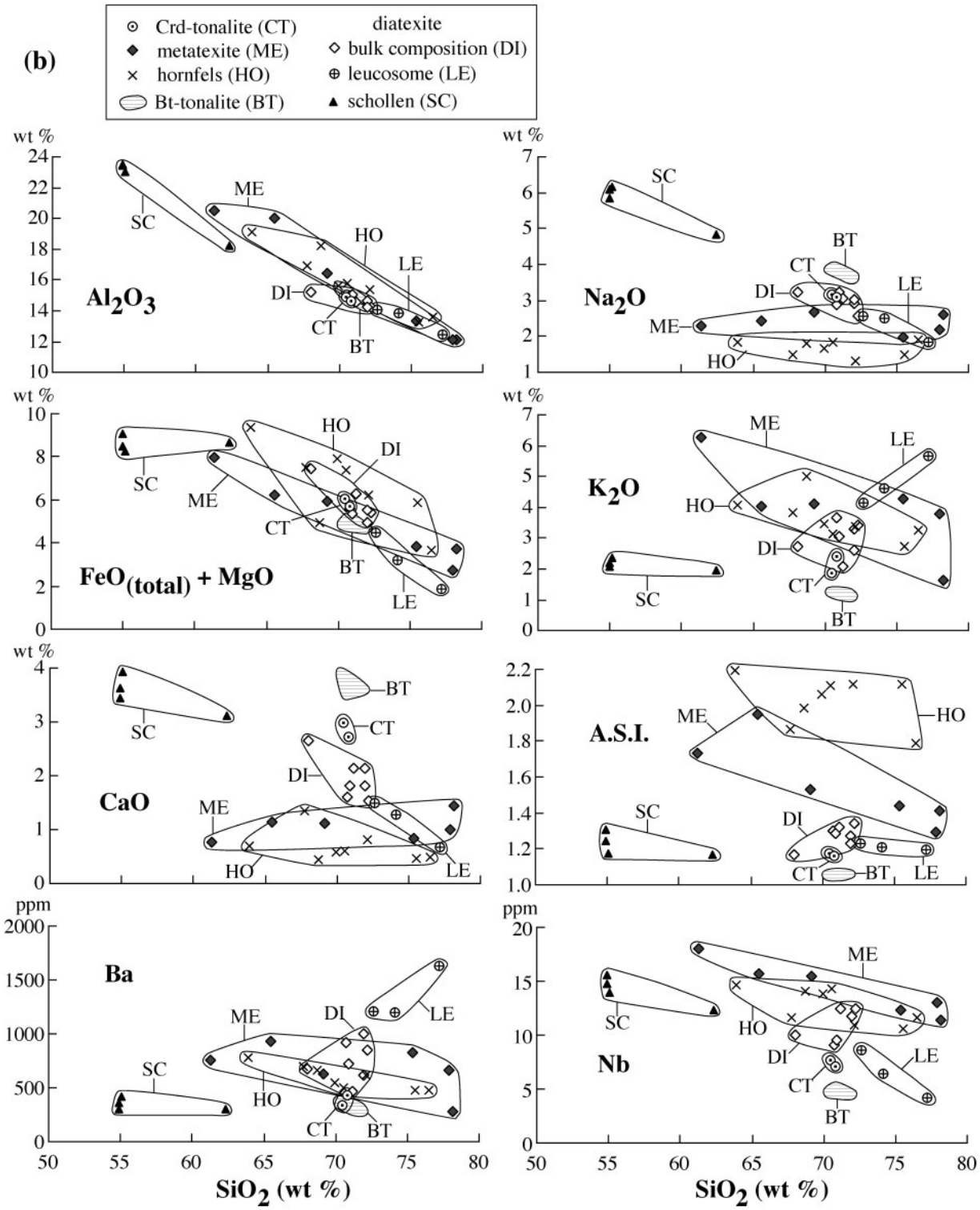


Fig. 10. Continued.

Downloaded from http://petrology.oxfordjournals.org/ by guest on June 28, 2012

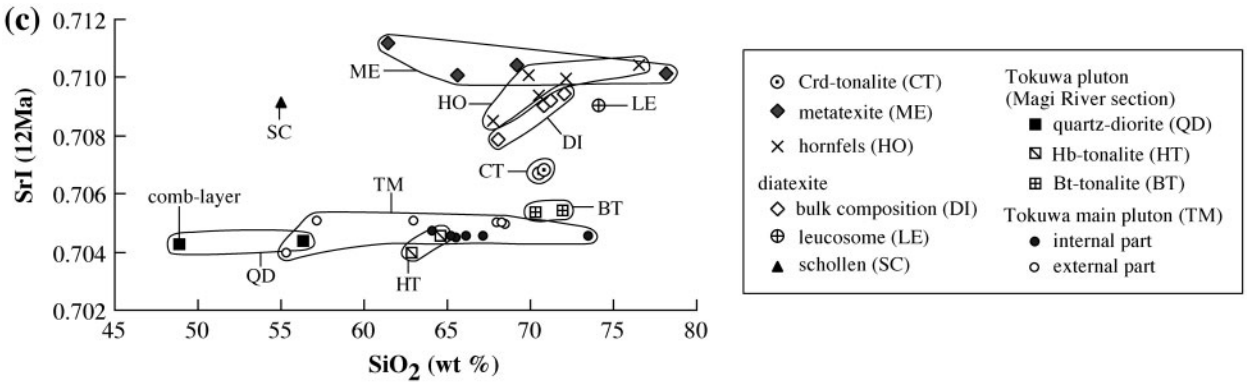


Fig. 10. Continued.

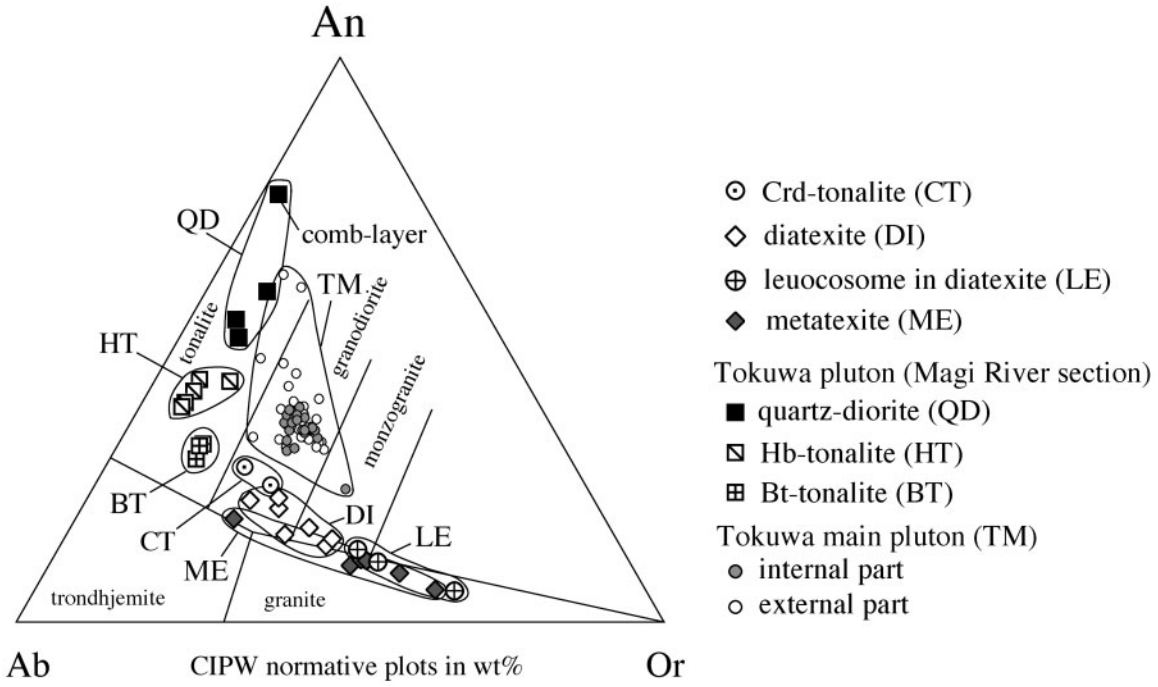


Fig. 11. An–Ab–Or normative ternary diagrams for the Crd-tonalite, diatexite, metatexite and granitoids in the Tokuwa pluton. The classification of granitoids is after Barker (1979).

trace element contents of the quartz-diorite are characterized by negative trends vs SiO_2 for Al_2O_3, $FeO_{(total)} + MgO$ and CaO, and positive trends for Na_2O, K_2O, Ba and Nb (Fig. 10a).

Compared with the granitoids in the Tokuwa main pluton, the Hb-tonalite is characterized by higher Na_2O and lower K_2O at a given SiO_2 content. It shows a decrease of Al_2O_3, $FeO_{(total)} + MgO$, CaO and Na_2O, but increases in K_2O, Ba and Nb with increasing SiO_2. The Bt-tonalite is characterized by a narrow range of compositional variation in most elements. It has higher Na_2O and lower K_2O contents at a given SiO_2 wt % than the Tokuwa main granite. The quartz-diorite and Hb-tonalite are metaluminous (A.S.I. 0·70–0·89 and 0·86–0·97, respectively) and their SrI is in the range 0·7043–0·7044 and 0·7040–0·7045, respectively. The Bt-tonalite, in contrast, is slightly peraluminous (1·05) and characterized by higher SrI (0·7054) compared with the quartz-diorite and Hb-tonalite (Fig. 10c).

Hornfels and metatexite

The hornfels (64–77 wt % SiO_2) are characterized by the following elemental variations and trends (Fig. 10b):

Downloaded from http://petrology.oxfordjournals.org/ by guest on June 28, 2012

a negative trend of Al_2O_3, $FeO_{(total)} + MgO$, K_2O, Ba and Nb vs SiO_2 and constant contents of CaO and Na_2O for variable SiO_2 ranges. They are strongly peraluminous (A.S.I. between 1·79 and 2·20) and their SrI ratio ranges from 0·7085 to 0·7104. The SiO_2 contents of the metatexites range from 61 to 78 wt %. Their Al_2O_3, $FeO_{(total)} + MgO$, K_2O, Ba and Nb contents define negative correlations vs SiO_2, whereas Na_2O and CaO contents are almost constant across the range of SiO_2 contents. The whole-rock compositions of the metatexite are broadly comparable with those of the hornfels except for differences in Na_2O and A.S.I., suggesting that the metatexite preserves most of the geochemical signature inherited from the hornfels. The metatexites have A.S.I. ranging from 1·29 to 1·94, which show a good negative correlation with SiO_2. The SrI of the metatexite ranges from 0·7100 to 0·7112.

Diatexite and Crd-tonalite

The SiO_2 content of the diatexite ranges from 68 to 72 wt %. Compared with the metatexite and hornfels, the diatexites contain lower amounts of Al_2O_3 and K_2O and higher CaO and Na_2O. Their A.S.I. (1·16–1·34) shows a positive correlation with SiO_2 but is lower than that of the metatexite and hornfelses. The SrI of the diatexite (0·7078–0·7094) is lower than that of the metatexite (0·7100 and 0·7112). The leucosomes (73–77 wt % SiO_2) are strongly peraluminous (A.S.I. 1·21–1·23) and enriched in K_2O and Ba, but depleted in Al_2O_3, $FeO_{(total)} + MgO$, CaO, Na_2O and Nb compared with the diatexite. The schollen, on other hand, have lower SiO_2 (55–62 wt %), K_2O and Rb, but higher Al_2O_3, $FeO_{(total)} + MgO$, CaO and Na_2O than the diatexite. Their A.S.I. ranges from 1·16 to 1·30. The SrI for the leucosome and the schollen is 0·7090 and 0·7091, respectively.

The Crd-tonalites (~71 SiO_2 wt %) are strongly peraluminous (A.S.I. 1·16–1·17) and belong to the 'S-type' granitoid affinity defined by Chappell & White (1974). They have intermediate compositions between the diatexite and the Bt-tonalite. Their Al_2O_3, $FeO_{(total)} + MgO$, Na_2O, and K_2O contents are comparable with those of the diatexite, although their CaO, Ba and Nb contents are intermediate between the diatexite and the Bt-tonalite. The SrI ratio of the Crd-tonalite ranges from 0·7067 to 0·7068, significantly higher than the values for the Bt-tonalite, but lower than those of the metatexite and diatexite.

DISCUSSION

Magmatic process in the Magi River section

The quartz-diorite, Hb-tonalite, and Bt-tonalite in the Magi River section (Fig. 2b) have comparable SrI ratios (0·7040–0·7054), suggesting that they are genetically related. The Hb-tonalite and quartz-diorite, most of which exhibit various types of cumulate texture, have nearly identical SrI ratios (0·7040–0·7045; Table 2). We attribute the lithological and chemical variations in these two rock types to crystal accumulation processes involving the mineral constituents in these rocks. The medium-grained homogeneous tonalite (MGZ-14c), which occurs 200 m from the intrusive contact (Loc. 1-c, Fig. 2b) lacks any cumulate texture (Fig. 6c). This rock is considered to represent the parental magma composition. A least-squares mass-balance calculation successfully explains the major-element compositional variation in the fine-grained Hb-tonalites and quartz-diorites by accumulation of Pl + Hb ± Bt from the assumed parental magma composition (MGZ-14c, Table 4; Fig. 12). The mineral compositions used for the least-squares mass-balance calculations are listed in Table 5.

Compositional variations in the Bt-tonalite can be explained by fractional crystallization processes ($F = 0·69–0·77$) involving removal of plagioclase, hornblende and biotite from the parental magma composition (MGZ-14c, Table 6; Fig. 12). However, the SrI of the Bt-tonalite (~0·7054) is slightly higher than that of the assumed parental magma composition (MGZ-14c, 0·7045), suggesting a significant role for country rock assimilation in its derivation. Assimilation and fractional crystallization (AFC) modeling of DePaolo (1981) was used to model the variations in whole-rock and SrI compositions in the Bt-tonalites. The hornfels (MKG-31a, Table 2) that occurs in the Magi River section (Loc. 1-d, Fig. 2b) was selected as a likely contaminant. The F value was estimated by a least-squares major-element mass-balance calculation (Table 5). The liquid–crystal partition coefficients used for this modeling are given in Table 7. The AFC modeling reproduces the whole-rock compositional variation in the Bt-tonalites well (Table 8). The r value (ratio of the mass of material assimilated to the mass of material crystallized) ranges from 0·37 to 0·44, corresponding to the assimilation of relatively small amounts of hornfels (10·3–11·3 wt %) into the fractionated melt.

The genetic link between the Hb-tonalite (marginal phase of the Tokuwa pluton) and the Tokuwa main pluton is more complex. The Sr-isotopic composition of the Hb-tonalite (0·7040–0·7045) is comparable with that of the Tokuwa main pluton (0·7040–0·7050), suggesting an insignificant role for country rock assimilation. Compared with the compositions of the Tokuwa main pluton, the Hb-tonalite has similar abundances of most elements except for distinctly lower K_2O and higher N_2O contents (Figs 10a and 11). Therefore, processes leading to a significant depletion in K_2O and enrichment in N_2O are necessary to derive the Hb-tonalite from the Tokuwa main pluton. We tested crystal fractionation models involving K-rich mineral(s), such as K-feldspar

Downloaded from http://petrology.oxfordjournals.org/ by guest on June 28, 2012

Table 4: Least-squares mass-balance calculations for accumulation modeling

Rock type:	Hb-tonalite				Quartz-diorite			
Sample no.:	MGZ-19	MGZ-20a	MGZ-23	MGZ-26	MGZ-09	MGZ-16c-1*	MGZ-16c-3	MGZ-17a
Model proportion (wt %)								
Albite	17·48	6·02	13·57	12·91	7·10	4·92	7·53	9·02
Anorthite	7·63	0·03	7·36	3·91	10·92	31·92	17·68	14·53
Hornblende	15·52	6·48	14·69	9·08	17·85	53·48	30·27	24·92
Biotite			0·90		4·79		10·52	4·71
Ilmenite	0·29	0·05	0·42		0·51	0·09	0·36	0·44
Apatite	0·19							
Parent magma†	58·89	87·42	63·05	74·09	58·82	9·59	33·64	46·37
Sum of R^2	0·05	0·22	0·09	0·09	0·07	0·19	0·24	0·13
Calculated composition								
SiO_2	60·70	63·96	60·70	62·86	58·02	48·88	53·14	56·29
TiO_2	0·64	0·56	0·75	0·49	0·94	0·64	1·08	0·91
Al_2O_3	16·93	16·16	16·90	16·84	17·27	18·18	17·53	17·43
FeO(total)	6·96	6·46	7·35	6·25	8·56	11·49	11·20	9·26
MnO	0·14	0·15	0·14	0·14	0·15	0·19	0·15	0·15
MgO	2·77	2·52	2·86	2·48	3·66	5·98	5·03	4·16
CaO	6·64	5·67	6·65	5·97	7·50	12·73	8·82	8·30
Na_2O	4·18	3·69	3·87	4·09	2·98	1·39	2·34	2·86
K_2O	0·81	1·12	0·94	0·97	1·15	0·38	1·31	1·03
P_2O_5	0·14	0·08	0·06	0·07	0·06	0·01	0·03	0·04
Total	99·91	100·37	100·21	100·15	100·28	99·87	100·64	100·43
Observed composition								
SiO_2	60·70	63·99	60·70	62·88	58·02	48·91	53·14	56·29
TiO_2	0·73	0·65	0·74	0·57	0·86	0·85	0·94	0·80
Al_2O_3	16·91	16·04	16·96	16·77	17·30	18·07	17·59	17·48
FeO(total)	6·87	6·38	7·36	6·17	8·64	11·27	11·34	9·37
MnO	0·17	0·15	0·17	0·15	0·19	0·21	0·21	0·19
MgO	2·94	2·48	2·96	2·51	3·58	6·19	4·87	4·04
CaO	6·66	5·81	6·53	6·06	7·43	12·86	8·71	8·22
Na_2O	4·17	3·69	3·76	4·09	2·92	1·40	2·24	2·79
K_2O	0·73	0·71	0·71	0·71	0·95	0·22	0·93	0·76
P_2O_5	0·11	0·10	0·10	0·09	0·10	0·01	0·03	0·07
Total	100·00	100·00	100·00	100·00	100·00	100·00	100·00	100·00

*Comb-layer.
†MGZ-14c (Table 2) was assumed as the parent magma composition.
R, residual for the calculations.

and/or biotite, to derive the Hb-tonalite composition from the Tokuwa main pluton; however, they resulted in considerably lower Al_2O_3 contents and A.S.I. values in the K-depleted differentiates that are not comparable with the Hb-tonalite composition (Fig. 10a).

In summary, the data suggest that the Hb-tonalite was injected in the marginal zone of the Tokuwa pluton. The quartz-diorite and Bt-tonalite are interpreted to have been derived from the Hb-tonalite magma by an accumulation process and an AFC process, respectively. We suggest that the Hb-tonalite is a distinct magma, unrelated to the Tokuwa main pluton by shallow-level magmatic differentiation processes.

Origin of metatexite, diatexite and Crd-tonalite

The metatexite at Loc. 1-a contains leucosomes composed of Kfs + Pl + Qtz + Bt + Crd ± Ms. This

Downloaded from http://petrology.oxfordjournals.org/ by guest on June 28, 2012

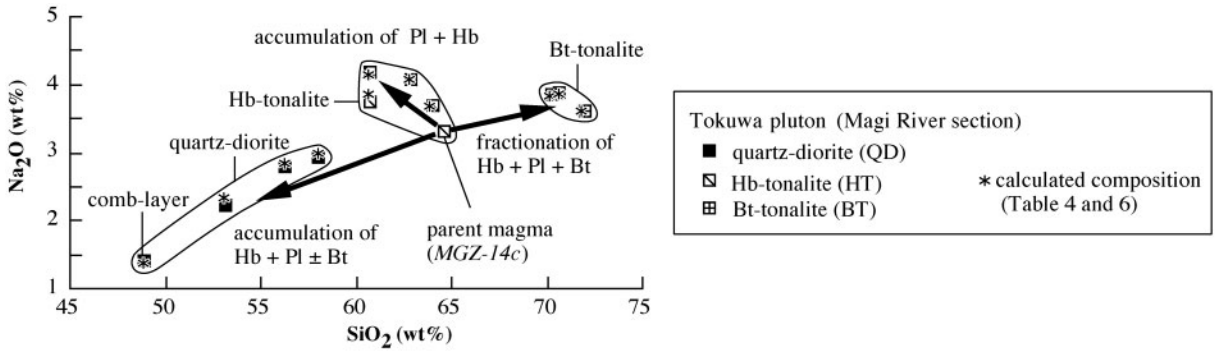


Fig. 12. SiO_2 vs Na_2O (wt %) showing the composition of the granitoids in the Magi River section in comparison with compositions calculated by the accumulation and fractionation model taking MGZ-14c as a parent magma (Tables 4 and 6). The observed compositions compare well with the calculated compositions.

Table 5: Mineral compositions used for the mass-balance modeling

	Albite	Anorthite	Hornblende*	Hornblende†	Biotite*	Biotite†	Ilmenite	Apatite
SiO_2	68·73	43·19	47·60	47·83	36·65	35·81		
TiO_2			1·18	1·02	4·01	3·95	50·00	
Al_2O_3	19·45	36·66	6·30	7·38	14·32	15·68		
FeO(total)			22·46	20·41	28·20	27·23	50·00	
MnO			0·33	0·34				
MgO			9·75	10·81	7·99	9·58		
CaO		20·16	10·70	10·79	0·17	0·27		57·00
Na_2O	11·82		1·11	0·93	0·38	0·42		
K_2O			0·57	0·49	8·29	7·04		
P_2O_5								43·00
Total	100·00	100·00	100·00	100·00	100·00	100·00	100·00	100·00

*Composition used for Hb-tonalite calculation.
†Composition used for Bt-tonalite and quartz-diorite calculation.

mineral assemblage is distinct from that of the granitoids in the Tokuwa pluton ($Pl + Qtz + Hb + Bt \pm Kfs$). Moreover, the SrI values of the leucosome-bearing metatexite are comparable with those of the hornfels and significantly higher than those of the Tokuwa pluton in the Magi River section (Hb-tonalite, Bt-tonalite and quartz-diorite, Fig. 10c), suggesting that the leucosome did not crystallize from a melt injected into the contact aureole from the Tokuwa magma.

Systematic variations exist between the whole-rock composition and SrI in the metatexite, diatexite and Crd-tonalite at Loc. 1-a. The CaO, Na_2O and K_2O contents and SrI ratio of the Crd-tonalite, diatexite, and metatexite are plotted as a function of distance from the Crd-tonalite outcrop in Fig. 13. From the metatexite through the diatexite to the Crd-tonalite, there is a systematic increase in CaO and Na_2O and decrease in K_2O and SrI. These trends clearly suggest that the Crd-tonalite and diatexite were formed by hybridization of the Tokuwa magma with the metatexite in variable proportions. We take an average composition of the metatexite as one end-member and an average composition of the Bt-tonalite as the other end-member, and evaluate a binary mixing model. The average Crd-tonalite and diatexite compositions plot along a mixing line between these two end-members in the SiO_2–SrI diagram (Fig. 14), suggesting that the Crd-tonalite and the diatexite were formed by hybridization between ~70 % of the Bt-tonalite and ~30 % of the metatexite, and ~30 % of the Bt-tonalite and ~70 % of the metatexite, respectively. Employing these proportions, major and trace element compositions were calculated for the mixed products, and are in excellent agreement with the measured whole-rock compositions (Fig. 15).

Downloaded from http://petrology.oxfordjournals.org/ by guest on June 28, 2012

Table 6: Least-squares mass-balance calculations for fractional crystallizition modeling

Rock type:	Bt-tonalite		
Sample no.:	MGZ-08a	MGZ-08b	MGZ-08c
Model composition (wt %)			
Albite	2·73	5·97	2·46
Anorthite	10·29	10·99	8·49
Hornblende	8·91	8·53	8·92
Biotite	2·86	5·04	3·38
Apatite		0·09	0·09
Residual melt	75·21	69·39	76·65
Sum of R^2	0·05	0·02	0·02
Calculated composition			
SiO_2	70·60	71·95	70·24
TiO_2	0·42	0·34	0·39
Al_2O_3	14·90	14·41	15·44
FeO(total)	4·09	3·68	3·82
MnO	0·16	0·17	0·15
MgO	1·21	1·07	1·12
CaO	3·49	3·56	3·83
Na_2O	3·85	3·61	3·82
K_2O	1·31	1·20	1·24
P_2O_5	0·13	0·08	0·07
Total	100·16	100·09	100·12
Observed composition			
SiO_2	70·62	71·97	70·26
TiO_2	0·49	0·47	0·44
Al_2O_3	14·90	14·41	15·43
FeO(total)	4·19	3·72	3·88
MnO	0·05	0·04	0·04
MgO	1·01	0·99	1·00
CaO	3·54	3·58	3·87
Na_2O	3·90	3·62	3·85
K_2O	1·22	1·12	1·22
P_2O_5	0·10	0·07	0·03
Total	100·00	100·00	100·00

MGZ-14c (Table 2) was assumed as the parent magma composition.
R, residual for the calculations.

Table 7: Trace element partition coefficients between mineral and liquid used for assimilation and fractional crystallization modeling

	Hornblende	Biotite	Plagioclase
Sr	0·022	0·120	2·840
Rb	0·014	3·260	0·048
Ba	0·044	6·360	0·308

Data are from Arth (1976) for dacitic and rhyolitic melt compositions.

Table 8: Assimilation and fractional crystallization modeling for Bt-tonalite

Sample no.:	MGZ-08b	MGZ-08c
DSr*	1·60	1·36
DRb*	0·57	0·50
DBa*	1·23	1·09
F	0·69	0·77
r	0·37	0·44
Calculated composition		
SrI	0·70542	0·70533
Sr (ppm)	151·5	178·5
Rb (ppm)	71·5	70·3
Ba (ppm)	268·1	287·9
Observed composition		
SrI	0·70542	0·70536
Sr (ppm)	174·3	198·4
Rb (ppm)	67·3	70·9
Ba (ppm)	288·5	378·4

MKG-31a (Table 2) was assumed as contaminant composition.
*Bulk partition coefficients for Sr, Rb and Ba.
F, fraction of remaining melt from Table 5; *r*, ratio of assimilation rate to fractional crystallization rate.

The hybridization model is supported by the heterogeneous appearance of the diatexite. The diatexite comprises a fine-grained migmatitic part having a granoblastic texture and a coarser-grained part with an equigranular and/or poikilitic texture, suggesting mixing of migmatite and injected melt in various proportions. The leucosome and schollen in the diatexite plot away from the mixing line (Fig. 14), suggesting that these were formed from the hybrid crystal mush by segregation processes and that they represent the extremes of solid-rich and melt-rich end-members of the hybrid diatexite magma.

The Crd-tonalite and diatexite both contain chemically zoned plagioclase crystals ($An_{18–95}$) with irregular-shaped calcic cores ($An_{70–95}$) (Fig. 5c–f). Similarly, the Bt-tonalite also has strongly zoned plagioclase ($An_{23–80}$), implying that injection of the Tokuwa magma might have introduced An-rich plagioclase crystals into the aureole migmatites and formed the An-rich cores found in the plagioclase in the diatexite and Crd-tonalite. Alternatively, the

Downloaded from http://petrology.oxfordjournals.org/ by guest on June 28, 2012

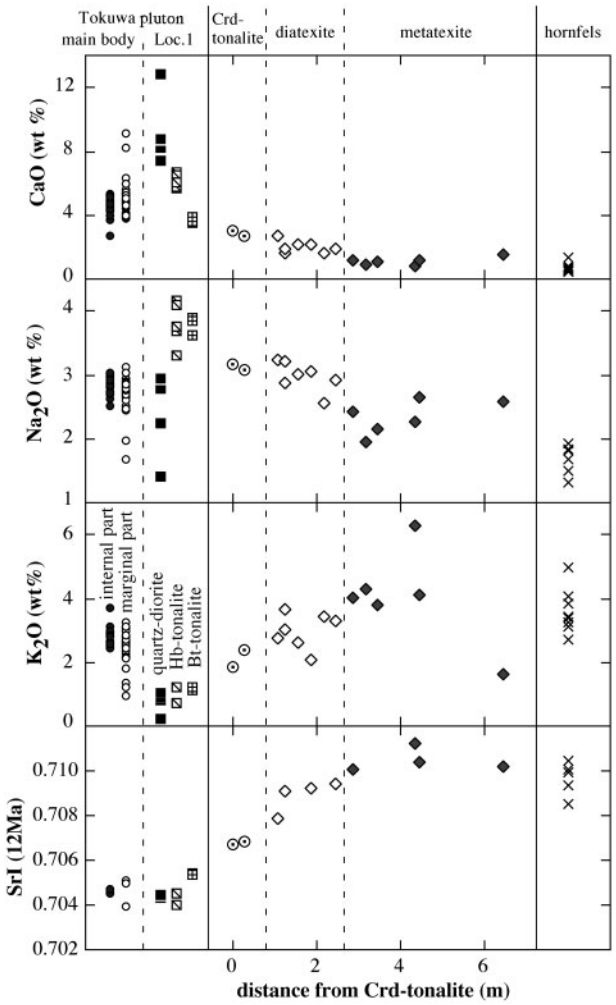


Fig. 13. CaO, Na_2O, K_2O and SrI compositions of the Crd-tonalite, diatexite and metatexite as a function of distance from the Crd-tonalite in Loc. 1-a. The compositions of hornfels and granitoids of the Tokuwa pluton are also given for comparison.

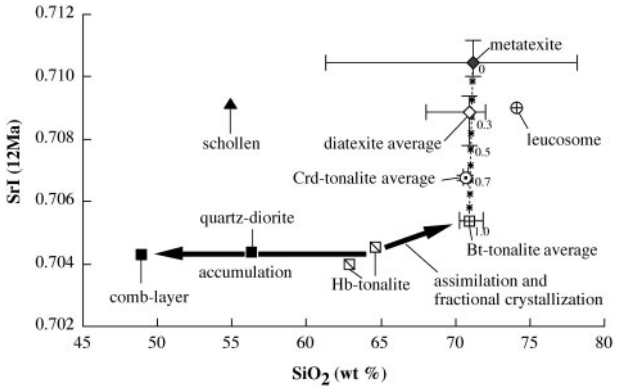


Fig. 14. SiO_2–SrI diagram for the rocks in the Magi River section. Average compositions of the metatexite, diatexite, Crd-tonalite and Bt-tonalite are indicated. Error bars represent the compositional range. The SrI of the quartz-diorite is nearly identical to that of the Hb-tonalite, suggesting the origin of the quartz-diorite from a parental Hb-tonalite magma. The Bt-tonalite was derived by assimilation and fractional crystallization of Hb-tonalite magma (Table 8). The Crd-tonalite and diatexite plot on a mixing line between the Bt-tonalite and metatexite.

An-rich cores in plagioclase might be residual crystals formed by anatexis. Plagioclase with similar morphology has been reported in a number of melting experiments (e.g. Tsuchiyama & Takahashi, 1983; Holtz & Johannes, 1991) and interpreted to represent a residual phase (restite) from partial melting of plagioclase-bearing rocks (Chappell *et al.*, 1987). Chemically zoned plagioclase crystals ($An_{18–90}$) are also present in the biotite-enriched clots enclosed in the diatexite. There is no firm evidence to suggest a hybrid origin for these clots. The clots contain biotite crystals with a sponge-like texture, suggesting that their formation was by melting reaction (8) in a sedimentary precursor (Fig. 5k and l). Therefore, some of the An-rich cores in plagioclase could have been formed by anatexis, and, therefore, represent a residual mineral.

Mechanism of hybridization at the intrusive contact

The data obtained during this study suggest that the diatexite and Crd-tonalite were formed at the interface between the Tokuwa pluton and the surrounding migmatites by variable degrees of mixing associated with crystal fractionation (Fig. 16). Magmatic stoping has been suggested as an important mechanism to produce the heterogeneous features of the Tokuwa pluton (Shimizu, 1986). This view is supported by our field observations in the external parts of Tokuwa pluton, such as the abundant occurrence of various-sized angular sedimentary xenoliths which we interpret as stoped blocks or fragments (Figs 6d and 16).

At the emplacement stage, the Tokuwa magma intruded into its sedimentary host-rocks, engulfing blocks and fragments derived from the roof-rocks (Fig. 16a). Solidification of the magma started from the outermost margin of the magma chamber and formed a solidified crust (Fig. 16a). The solidifying magma supplied conductive and latent heat outwards into the adjacent country rocks that culminated in the formation of anatectic melts in the contact aureole (Fig. 16a). Fractional crystallization of the Tokuwa magma in association with host-rock assimilation formed the Bt-tonalite magma in the roof portion of the magma chamber (Fig. 16a and b). The early solidified crust collapsed and dropped into the magma chamber under gravitational forces (Fig. 16b). The space formed at the margin after this gravitational collapse provided a low-pressure region at the Tokuwa magma–wall-rock interface where a further invasion of magma into the country rocks (Fig. 16b) could occur. It was the Bt-tonalite magma

Downloaded from http://petrology.oxfordjournals.org/ by guest on June 28, 2012

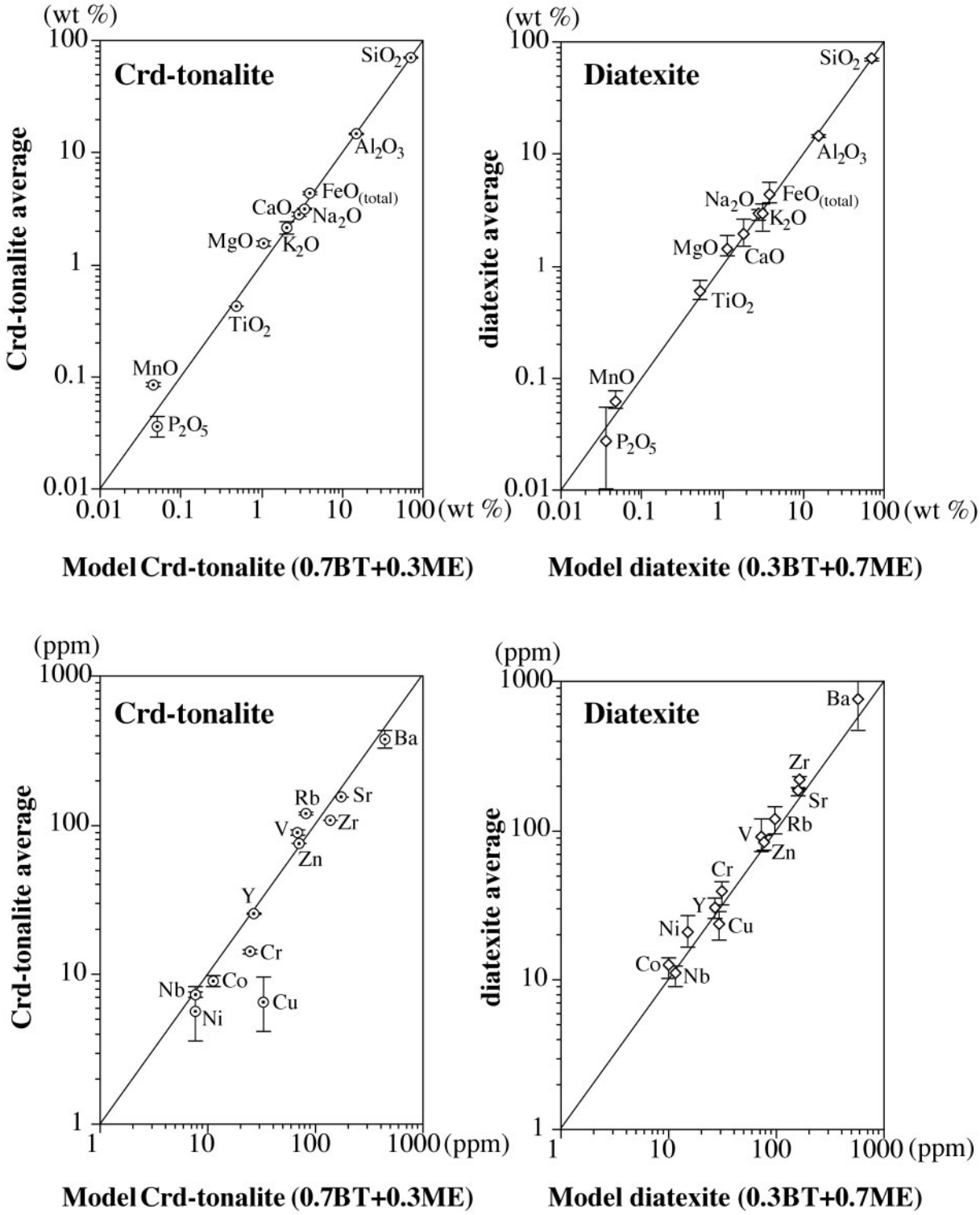


Fig. 15. Comparisons of major and trace element abundances of the calculated hybrid rock against the average composition of the Crd-tonalite (left) and diatexite (right). The model compositions of the Crd-tonalite and the diatexite are calculated by simple binary mixing of an average composition of the Bt-tonalite and an average composition of the metatexite (70% Bt-tonalite + 30% metatexite for the Crd-tonalite and 30% Bt-tonalite + 70% metatexite for the diatexite). The mixing ratio of the metatexite and Bt-tonalite is estimated from the SiO_2–SrI diagram (Fig. 14).

Downloaded from http://petrology.oxfordjournals.org/ by guest on June 28, 2012

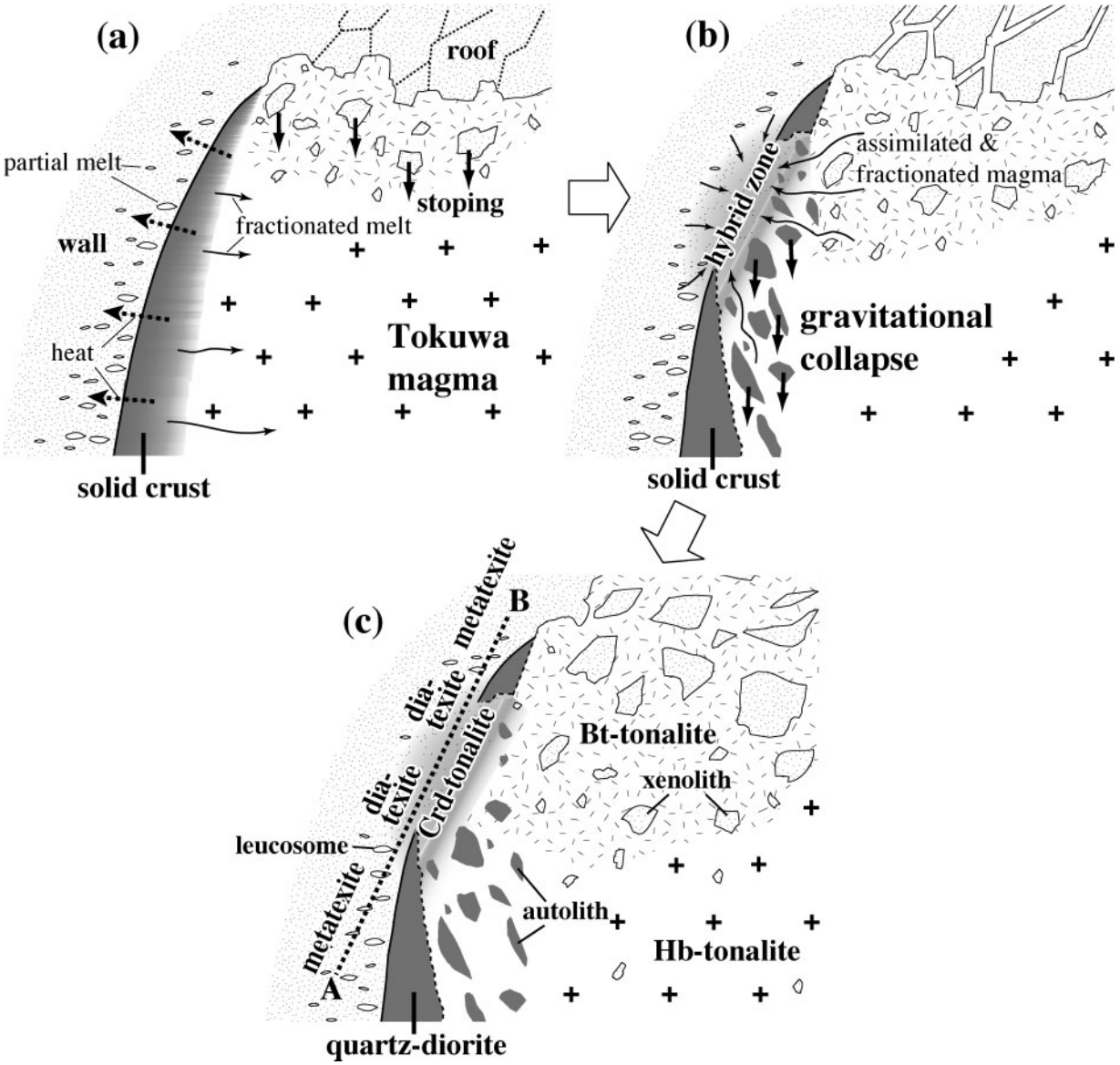


Fig. 16. Conceptual model explaining the generation of the Crd-tonalite, diatexite, metatexite and granitoids in the marginal parts of Tokuwa pluton as observed in the Magi River section. (a) Emplacement of the Tokuwa pluton associated with magmatic stoping. Magma emplacement gave rise to anatexis of host sedimentary rocks. Solidification of the Tokuwa magma started from the outermost margin of the magma chamber and formed a solid crust. Fractionated Tokuwa magma was slightly contaminated by hornfels. (b) The collapse of solid crust into the magma chamber by gravitational instability. The space formed after the gravitational collapse provided low-pressure regions along the Tokuwa magma–wall-rock interface, which allowed the injection of fractionated and contaminated magma into the partially melted host-rocks to form hybrid magma. (c) Solidification of the Tokuwa magma, hybrid magma and partially melted host-rocks. The hybrid magma formed the Crd-tonalite and the diatexite. The partially melted host-rocks formed metatexite. The fractionated and contaminated magma formed the Bt-tonalite. The early crystallized solid crust is recognized as quartz-diorite and/or hornblende-rich autoliths in the Tokuwa pluton. Dashed line A–B represents the present surface corresponding to that of Figs 2b and 7a.

that migrated into the low-pressure region and mixed with the partially melted host-rocks (metatexite) and produced the Crd-tonalite and diatexite by hybridization. The quartz-diorite has a cumulate and comb-layering structure and may represent the earlier crystallized solid crust (Fig. 16c), because crystallizing magma at the wall region may squeeze its residual melt into the inside of the magma chamber (Fig. 16a). A relatively mafic rock with a cumulate texture (MKG-05b, 55 wt % SiO_2) occurs in the Tokuwa main pluton about 1 km NNE from Loc. 1-a. This sample has an SrI (0·7040) close to that of the quartz-diorite (0·7043–0·7044), and might, therefore, represent a remnant of the solid crust that sank downwards within the magma chamber (Fig. 16c).

Downloaded from http://petrology.oxfordjournals.org/ by guest on June 28, 2012

Various petrogenetic models for the formation of cordierite-bearing 'S-type' granitoids have been proposed: (1) anatexis of peraluminous metasedimentary rooks (e.g. Chappell *et al.*, 1987); (2) hybridization of mantle-derived magma and crustal rocks (e.g. Barbarin, 1996; Castro *et al.*, 1999; Sandeman & Clarke, 2003; Healy *et al.*, 2004); (3) assimilation of sedimentary wall-rocks by a metaluminous to weakly peraluminous granitoid magma during emplacement (e.g. Ugidos & Recio, 1993; Fourcade *et al.*, 2001). In contrast to the first two processes, which can produce large volumes of primary 'S-type' magma, the last process forms only a small volume of cordierite-bearing granitoid by interaction between the granitoid magmas and its host-rocks, as suggested for the Tokuwa pluton.

In this study we clearly demonstrate that even relatively low-temperature, shallow-level, granitoid plutons can cause the formation of migmatites and magma–migmatite interactions at the intrusive contact. Castro *et al.* (2003) described extensive interactions between mafic magma and crustal anatectic rocks in the Sanabria appinite–migmatite complex, NW Iberian Massif, Spain. They suggested that water-rich fluids were released from a crystallizing basaltic magma through its chilled margin along fractures, or by intergranular diffusion, into the exterior migmatites. They further suggested that interaction between the fluids and the surrounding migmatites generated a diverse range of rocks from monzodiorite to granodiorite and to leucogranite in the region of anatexis. In addition, Castro (2003) proposed a new genetic model for granitic rocks in the Lewisian complex, Scotland. He suggested that the invasions of crustal regions by andesitic magmas derived from a subduction-modified mantle wedge supplied fluids necessary for crustal melting and granite generation.

In our study of the Tokuwa pluton we highlight the formation of hybrid 'S-type' granite magma in the anatectic zone surrounding a granitoid pluton. We suggest that gravitational collapse of a portion of the crystallized wall of the magma chamber is one of the important conditions driving invasion of granitoid magma into the surrounding anatectic region (contact aureole), and consequent formation of hybrid rocks.

In contrast to studies of granitoids within ancient orogenic belts where the details of their petrogenesis are often disguised by extensive later deformation, young granitoids such as the Tokuwa pluton provide us with clear information on not only the petrogenesis but also the tectonic setting. Our results contribute to a better understanding of the petrogenetic processes involved in the formation of cordierite-bearing 'S-type' granitoids in contact-aureoles reported from various ancient orogenic belts (e.g. White & Chappell, 1988). It has been suggested by previous workers that the tectonic setting of arc–arc collision and arc accretion in the Izu Collision Zone, where the Tokuwa pluton is located, is similar to that of ancient (Archaean) orogenic belts (e.g. Taira *et al.*, 1992). Therefore, the example of the Tokuwa pluton may be relevant to many ancient orogenic belts, especially those related to arc collision settings.

CONCLUSIONS

Migmatites and Crd-bearing tonalites are developed in the contact aureole of the Miocene Tokuwa pluton. The mineral paragenesis and textures in these rocks suggest the following low-pressure sub-solidus and melting reactions towards the intrusive contact: $Qtz + Chl + Ms = Crd + Bt + H_2O$, $Qtz + Bt + Ms = Crd + Kfs + H_2O$, $Qtz + Ms = Als + Kfs + H_2O$, And = Sil, $Ms = Crn + Kfs + H_2O$, $Kfs + Qtz + Pl + H_2O = L$, Qtz + Ms + Mg-rich Bt = L + Crd + Fe-rich Bt, Qtz + Ms + Na-rich Pl + Mg-rich Bt = L + Ca-rich Pl + Fe-rich Bt + Crd. Peak metamorphic P–T conditions of ~3 kbar and ~780°C are estimated for the garnet-bearing metatexite in the contact aureole, suggesting an emplacement depth of ~10 km for the Tokuwa pluton. A wide range of petrographic, geochemical and Sr-isotopic variations is identified in the marginal part of the Tokuwa pluton adjacent to the contact aureole (Magi River section). These variations suggest that the marginal parts of the pluton were formed by crystal accumulation and fractionation processes associated with a limited degree of assimilation of country rocks (~10 wt % assimilation). The geochemical and Sr-isotopic data suggest that the Crd-tonalite and the diatexite in the contact aureole were formed by hybridization of the Tokuwa magma with the host anatectic metasedimentary rocks. Gravitational collapse of early crystallized solid crust into the magma chamber permitted the hybridization of the granitoid magma with the partially melted host-rocks of the contact-aureole.

ACKNOWLEDGEMENTS

We thank E. W. Sawyer, M. Obata, A. Patiño-Douce and two anonymous reviewers for their helpful comments and suggestions for improvement on an earlier version of this manuscript. The authors also wish to thank Y. Kaneko, D. Prakash, R. Mazumder, H. Kamiyama, T. Kawakami and J. Kokonyangi for valuable discussion and comments. K. Shiraishi, Y. Motoyoshi and K. Seno are acknowledged for their analytical support. This work was partly supported by JSPS Grant-in-Aid for Scientific Research (12440147, 13373005) to M.A., and a Sasakawa Scientific Research Grant from the Japan Science Society (14-305) to S.S.

Downloaded from http://petrology.oxfordjournals.org/ by guest on June 28, 2012

REFERENCES

Aoike, K. (1999). Tectonic evolution of the Izu collision zone. *Research Report of the Kanagawa Prefectural Museum, Natural History* **9**, 111–151 (in Japanese with English abstract).

Arth, J. G. (1976). Behaviour of trace elements during magmatic processes—a summary of theoretical models and their applications. *Journal of Research of the US Geological Survey* **4**, 41–47.

Barbarin, B. (1996). Genesis of the two main types of peraluminous granitoids. *Geology* **24**, 295–298.

Barker, F. (1979). Trondhjemite: definition, environment and hypotheses of origin. In: Barker, F. (ed.) *Trondhjemites, Dacites and Related Rocks*. Amsterdam: Elsevier, pp. 1–12.

Bea, F. (1991). Geochemical modeling of low melt-fraction anatexis in peraluminous system: the Pena Negra Complex (central Spain). *Geochimica et Cosmochimica Acta* **55**, 1859–1874.

Berman, R. G. (1991). Thermobarometry using multi-equilibrium calculations: a new technique, with petrological applications. *Canadian Mineralogist* **29**, 833–855.

Berman, R. G. & Aranovich, L. Ya. (1996). Optimized standard state and solution properties of minerals. 1. Model calibration for olivine, orthopyroxene, cordierite, garnet, and ilmenite in the system FeO–MgO–CaO–Al_2O_3–TiO_2–SiO_2. *Contributions to Mineralogy and Petrology* **126**, 1–24.

Brown, M. (1973). The definition of metatexis, diatexis and migmatite. *Proceedings of the Geologists' Association* **84**, 371–382.

Castro, A. (2003). The source of granites: inferences from the Lewisian complex. *Scottish Journal of Geology* **40**, 49–65.

Castro, A., Patiño Douce, A. E., Corretge, L. G., De La Rosa, J. D., El-Bird, M. & El-Hmidi, H. (1999). Origin of peraluminous granites and granodiorites, Iberian massif, Spain. An experimental test of granite petrogenesis. *Contributions to Mineralogy and Petrology* **135**, 255–276.

Castro, A., Corretge, L. G., De la Rosa, J. D., Fernandez, C., Lopez, S., Garcia-Moreno, O. & Chacon, H. (2003). The appinite–migmatite complex of Sanabria, NW Iberian massif, Spain. *Journal of Petrology* **44**, 1309–1344.

Chappell, B. W. & White, A. J. R. (1974). Two contrasting granite types. *Pacific Geology* **8**, 173–174.

Chappell, B. W., White, A. J. R. & Wyborn, D. (1987). The importance of residual source material (restite) in granite petrogenesis. *Journal of Petrology* **28**, 1111–1138.

Chatterjee, N. D. & Froese, E. F. (1975). A thermodynamic study of the pseudobinary join muscovite–paragonite in the system $KAlSi_3O_8$–$NaAlSi_3O_8$–Al_2O_3–SiO_2–H_2O. *American Mineralogist* **60**, 985–993.

DePaolo, D. J. (1981). Trace element and isotopic effects of combined wallrock assimilation and fractional crystallization. *Earth and Planetary Science Letters* **53**, 189–202.

Fourcade, S., Capdevila, R., Ouabadi, A. & Martineau, F. (2001). The origin and geodynamic significance of the Alpine cordierite-bearing granitoids of northern Algeria. A combined petrological, mineralogical, geochemical and isotopic (O, H, Sr, Nd) study. *Lithos* **57**, 187–216.

Greenfield, J. E., Clark, G. L., Bland, M. & Clark, D. J. (1996). *In-situ* migmatite and hybrid diatexite at Mt. Stafford, central Austria. *Journal of Metamorphic Geology* **14**, 413–426.

Healy, B., Collins, W. J. & Richards, S. W. (2004). A hybrid origin for Lachlan S-type granites: the Murrumbidgee Batholith example. *Lithos* **78**, 197–216.

Holness, M. B. & Clemens, J. D. (1999). Partial melting of the Appin Quartzite driven by fracture-controlled H_2O infiltration in the aureole of the Ballachulish Igneous Complex, Scottish Highlands. *Contributions to Mineralogy and Petrology* **136**, 154–168.

Holtz, F. & Johannes, W. (1991). Genesis of peraluminous granite I. Experimental investigation of melt compositions at 3 and 5 kbar and various H_2O activities. *Journal of Petrology* **32**, 935–958.

Ishihara, S. (1977). The magnetite and ilmenite series in granitic rocks. *Mining Geology* **27**, 293–305.

Johannes, W. & Holtz, F. (1996). *Petrogenesis and Experimental Petrology of Granitic Rocks*. Berlin: Springer, 335 pp.

Kawano, Y. & Ueda, Y. (1966). K–Ar dating on the igneous rocks in Japan (IV)—granitic rocks in the northeastern Japan. *The Journal of the Japanese Association of Mineralogist, Petrologist and Economic Geologist* **56**, 191–211 (in Japanese).

Kretz, R. (1983). Symbols for rock-forming minerals. *American Mineralogist* **68**, 277–279.

LeBas, M. J. & Streckeisen, A. L. (1991). The IUGS systematics of igneous rocks. *Journal of the Geological Society, London* **148**, 825–833.

Marchildon, N. & Brown, M. (2001). Melt segregation in late syn-tectonic anatectic migmatites: an example from the Onawa contact aureole, Maine, USA. *Physics and Chemistry of the Earth (A)* **26**, 225–229.

Mehnert, K. R. (1968). *Migmatites and the Origin of Granitic Rocks*. Amsterdam: Elsevier, 393 pp.

Moore, J. G. & Lockwood, J. P. (1973). Origin of comb layering and orbicular structure, Sierra Nevada Batholith, California. *Geological Society of America Bulletin* **84**, 1–20.

Motoyoshi, Y. & Shiraishi, K. (1995). Quantitative chemical analyses of rocks with X-ray fluorescence analyzer: (1) Major elements. *Nankyoku Shiryo (Antarctic Record)* **39**, 40–48 (in Japanese with English abstract and figure captions).

Motoyoshi, Y., Ishizuka, H. & Shiraishi, K. (1996). Quantitative chemical analyses of rocks with X-ray fluorescence analyzer: (2) Trace elements. *Nankyoku Shiryo (Antarctic Record)* **40**, 53–63 (in Japanese with English abstract and figure captions).

Nakajima, T., Shirahase, T. & Shimata, K. (1990). Along-arc lateral variation of Rb–Sr and K–Ar ages of Cretaceous granitic rocks in Southwest Japan. *Contributions to Mineralogy and Petrology* **104**, 381–389.

Niitsuma, N. (1989). Collision tectonics in the South Fossa magna, central Japan. *Modern Geology* **14**, 3–18.

Ogawa, Y., Seno, T., Tokuyama, H., Akiyoshi, H., Fujioka, K. & Taniguchi, H. (1989). Structure and development of the Sagami trough and the Boso triple junction. *Tectonophysics* **160**, 135–150.

Ozaki, M., Makimoto, H., Sugiyama, Y., Mimura, K., Sakai, A., Kubo, K., Kato, H., Komazawa, M., Hiroshima, T. & Sudo, S. (2002). *Geological map of Japan 1:200,000, Kofu*. Tsukuba: Geological Survey of Japan, AIST (in Japanese with English abstract and figure captions).

Pattison, D. R. M. (1992). Stability of andalusite and sillimanite and the Al_2SiO_5 triple point: constraints from the Ballachulish aureole, Scotland. *Journal of Geology* **100**, 423–446.

Pattison, D. R. M. & Harte, B. (1988). Evolution of structurally contrasting anatectic migmatites in the 3-kbar Ballachulish aureole, Scotland. *Journal of Metamorphic Geology* **6**, 475–494.

Pattison, D. R. M. & Harte, B. (1997). The geology and evolution of the Ballachulish Igneous Complex and Aureole. *Scottish Journal of Geology* **33**, 1–29.

Saito, K., Kato, K. & Sugi, S. (1997). K–Ar dating studies of Ashigawa and Tokuwa granodiorite bodies and plutonic geochronology in the South Fossa Magna, central Japan. *The Island Arc* **6**, 158–167.

Saito, S., Arima, M., Nakajima, T. & Kimura, J.-I. (2004). Petrogenesis of Ashigawa and Tonogi granitic intrusions, southern

Downloaded from http://petrology.oxfordjournals.org/ by guest on June 28, 2012

part of the Miocene Kofu Granitic Complex, central Japan: M-type granite in the Izu arc collision zone. *Journal of Mineralogical and Petrological Sciences* **99**, 104–117.

Sandeman, H. A. & Clarke, A. H. (2003). Glass-rich, cordierite–biotite rhyodacite, Valle Ninahuisa, Puno, SE Peru: petrological evidence for hybridization of 'Lachlan S-type' and potassic mafic magmas. *Journal of Petrology* **44**, 355–385.

Sato, K. (1991). Miocene granitoid magmatism at the island-arc junction, central Japan. *Modern Geology* **15**, 367–399.

Sato, K. & Ishihara, S. (1983). Chemical composition and magnetic susceptibility of the Kofu granitic complex. *Bulletin of the Geological Survey of Japan* **34**, 413–427 (in Japanese with English abstract and figure captions).

Sawyer, E. W. (1996). Melt segregation and magma flow in migmatites: implications for the generation of granite magmas. *Transactions of the Royal Society of Edinburgh: Earth Sciences* **87**, 85–94.

Sawyer, E. W. (1999). Criteria for the recognition of partial melting. *Physics and Chemistry of the Earth (A)* **24**, 269–279.

Shibata, K., Kato, Y. & Mimura, K. (1984). K–Ar ages of granites and related rocks from the northern Kofu area. *Bulletin of the Geological Survey of Japan* **35**, 19–24 (in Japanese with English abstract).

Shimizu, M. (1986). The Tokuwa batholith, central Japan—an example of ilmenite-series and magnetite-series granitoids in a batholith. *University Museum, University of Tokyo, Bulletin* **28**, 1–145.

Soh, W., Pickering, K. T., Taira, A. & Tokuyama, H. (1991). Basin evolution in the arc–arc Izu collision zone, Mio-Pliocene Miura Group, central Japan. *Journal of the Geological Society, London* **148**, 317–330.

Symmes, G. H. & Ferry, J. M. (1995). Metamorphism, fluid flow and partial melting in pelitic rocks from the Onawa contact aureole, central Maine, USA. *Journal of Petrology* **36**, 587–612.

Taira, A., Tokuyama, H. & Soh, W. (1989). Accretion tectonics and evolution of Japan. In: Ben-Avraham, Z. (ed.) *The Evolution of the Pacific Ocean Margins*. New York: Oxford University Press, pp. 100–123.

Taira, A., Pickering, K. T., Windley, B. F. & Soh, W. (1992). Accretion of Japanese island arcs and implications for the origin of Archean greenstone belts. *Tectonics* **11**, 1224–1244.

Takahashi, M. (1989). Neogene granitic magmatism in the South Fossa Magna collision zone, central Japan. *Modern Geology* **14**, 127–143.

Takahashi, M. & Saito, K. (1997). Miocene intra-arc bending at an arc–arc collision zone, central Japan. *The Island Arc* **6**, 168–182.

Tsuchiyama, A. & Takahashi, E. (1983). Melting kinetics of a plagioclase feldspar. *Contributions to Mineralogy and Petrology* **84**, 345–354.

Ugidos, J. M. & Recio, C. (1993). Origin of cordierite-bearing granites by assimilation in the Central Iberian Massif, Spain. *Chemical Geology* **103**, 27–43.

Vernon, R. H. & Collins, W. J. (1988). Igneous microstructures in migmatites. *Geology* **16**, 1126–1129.

White, A. J. R. & Chappell, B. W. (1988). Some supracrustal (S-type) granites of the Lachlan Fold Belt. *Transactions of the Royal Society of Edinburgh: Earth Sciences* **79**, 169–181.

Yamada, Y., Kohno, H., Shiraki, K., Nagano, T., Kakubuchi, S., Oba, T., Kawate, S. & Murata, M. (1997). Analysis of major, trace and rare earth elements in geological samples using low dilution glass bead. *Advances in X-ray Chemical Analysis, Japan* **29**, 47–70 (in Japanese with English abstract).

Zeng, L., Saleeby, J. B. & Asimow, P. (2005*a*). Nd isotope disequilibrium during crustal anatexis: a record from the Goat Ranch migmatite complex, southern Sierra Nevada batholith, California. *Geology* **33**, 53–56.

Zeng, L., Saleeby, J. B. & Ducea, M. (2005*b*). Geochemical characteristics of crustal anatexis during the formation of migmatite at the Southern Sierra Nevada, California. *Contributions to Mineralogy and Petrology* **150**, 386–402.

Downloaded from http://petrology.oxfordjournals.org/ by guest on June 28, 2012